Nucleic Acids Research, 2024, **52**, 6376–6391
https://doi.org/10.1093/nar/gkae317
Advance access publication date: 9 May 2024
Genome integrity, repair and replication

EXO1 and DNA2-mediated ssDNA gap expansion is essential for ATR activation and to maintain viability in BRCA1-deficient cells

Néstor García-Rodríguez [1,2,*], Iria Domínguez-García[1,2], María del Carmen Domínguez-Pérez[1,2] and Pablo Huertas [1,2,*]

[1]Centro Andaluz de Biología Molecular y Medicina Regenerativa (CABIMER), Universidad de Sevilla-CSIC-Universidad Pablo de Olavide, Sevilla, Spain
[2]Departamento de Genética, Universidad de Sevilla, Sevilla, Spain

*To whom correspondence should be addressed. Tel: +34 954 467 667; Fax: +34 954 461 664; Email: phuertas@us.es
Correspondence may also be addressed to Néstor García-Rodríguez. Tel: +34 95 446 2139; Fax: +34 954 461 664; Email: ngarcia@us.es

Abstract

DNA replication faces challenges from DNA lesions originated from endogenous or exogenous sources of stress, leading to the accumulation of single-stranded DNA (ssDNA) that triggers the activation of the ATR checkpoint response. To complete genome replication in the presence of damaged DNA, cells employ DNA damage tolerance mechanisms that operate not only at stalled replication forks but also at ssDNA gaps originated by repriming of DNA synthesis downstream of lesions. Here, we demonstrate that human cells accumulate post-replicative ssDNA gaps following replicative stress induction. These gaps, initiated by PrimPol repriming and expanded by the long-range resection factors EXO1 and DNA2, constitute the principal origin of the ssDNA signal responsible for ATR activation upon replication stress, in contrast to stalled forks. Strikingly, the loss of EXO1 or DNA2 results in synthetic lethality when combined with BRCA1 deficiency, but not BRCA2. This phenomenon aligns with the observation that BRCA1 alone contributes to the expansion of ssDNA gaps. Remarkably, BRCA1-deficient cells become addicted to the overexpression of *EXO1, DNA2* or *BLM*. This dependence on long-range resection unveils a new vulnerability of BRCA1-mutant tumors, shedding light on potential therapeutic targets for these cancers.

Graphical abstract

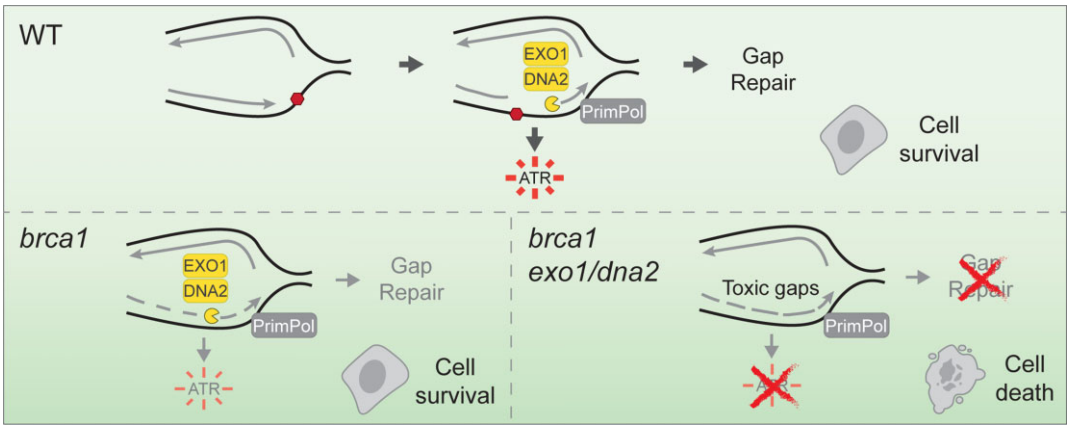

Introduction

The genetic information encoded by DNA is under constant threat from various internal and external sources of stress. One particularly vulnerable situation occurs during the process of DNA replication, where the replication machinery faces numerous obstacles that can lead to what is known as 'replication stress' (1). Stalling of the replication forks results in the formation of stretches of single-stranded DNA (ssDNA), likely as a consequence of the uncoupling of helicase and polymerase activities or leading and lagging strand synthesis. The persistent accumulation of ssDNA, bound by Replication Protein A (RPA), triggers the activation of the replication stress response, primarily mediated by the kinase ataxia-telangiectasia and Rad3-related (ATR) (2). Once ATR is activated, it phosphorylates the effector kinase CHK1, which modulates the checkpoint re-

Received: October 6, 2023. **Revised:** March 25, 2024. **Editorial Decision:** April 9, 2024. **Accepted:** May 2, 2024

sponse that ultimately leads to cell cycle arrest and DNA repair (3).

To allow the resumption of DNA replication in case of fork stalling, cells have evolved DNA damage tolerance (DDT) mechanisms. These mechanisms ensure the complete replication of the genome while preventing the deleterious consequences of prolonged fork stalling such as fork collapse and, ultimately, genome instability and/or cell death (4,5). One of the DDT mechanisms is known as translesion DNA synthesis (TLS), which employs Y-family DNA polymerases (Polη, Polι, Polκ and REV1). These specialized polymerases are able to bypass DNA lesions by inserting nucleotides opposite the damaged site, albeit in a potentially error-prone manner. Following this insertion step, DNA is extended by the B-family DNA polymerase Polζ, composed of REV3L, REV7, POLD2 and POLD3 (6,7). Another mechanism of DDT is template switching (TS), an error-free recombinational process that uses the nascent DNA daughter strand on the sister chromatid as a temporary template to bypass the DNA lesion (5). Moreover, stalled replication forks can undergo a structural rearrangement known as replication fork reversal, where the two daughter strands anneal, leading to the formation of a four-way junction structure (5). Fork reversal serves to impede fork collapse while also triggering TS by enabling the blocked 3′end to use the complementary daughter strand for DNA extension beyond the point of stalling. In addition to TLS or TS at the fork, a third mechanism of DDT involves the re-initiation of DNA synthesis beyond the lesion through repriming. This mechanism leads to the formation of an unreplicated ssDNA gap behind the advancing fork, which subsequently need to be filled in a post-replicative manner through either TLS or TS, a process known as gap filling or post-replication repair (8–15). In vertebrates, repriming is thought to be catalyzed by the Primase-Polymerase PrimPol (16–18). How cells choose among the different DDT pathways is currently under active investigation. In budding yeast, it has been recently shown that most of the ssDNA signal accumulating during replication upon methyl methanesulfonate (MMS) or ultraviolet (UV) damage arises at post-replicative regions, thus suggesting repriming as a predominant mechanism of DDT (19). Differently from budding yeast, replication fork reversal, detected by electron microscopy, was found to be a global response to replication challenges in mammalian cells (20). However, recent studies have confronted this model by revealing that the response to genotoxic stress varies depending on factors such as the nature or dosage of the replication challenge (4,21). In this regard, the formation of ssDNA gaps through repriming has been observed in mammalian cells following the induction of a wide range of DNA lesions, including bulky adducts (22,23) or DNA interstrand crosslinks (24,25), and even upon other sources of replication stress that do not induce DNA damage, such as the depletion of nucleotide pools, inhibition of PARP1, or DNA secondary structures (26–28).

The coordination between checkpoint signaling and fork restart mechanisms is poorly understood. The extent of fork uncoupling can be limited by repriming events that can reduce the exposure of ssDNA at forks. This activity is expected to hinder the activation of the checkpoint, which requires a critical number of arrested forks (29,30). In yeast, it has been observed that the ssDNA signal triggering the activation of the replication checkpoint upon replisome-stalling lesions primarily originates from the expansion of post-replicative gaps rather than directly form the fork (31). However, it is yet to be determined whether checkpoint signaling also arises from gaps in human cells.

Replication gaps have emerged as a potential vulnerability in cancer cells (21,26,32). Intriguingly, deficiencies in the hereditary breast cancer genes, *BRCA1* and *BRCA2*, have been found to result in the accumulation of ssDNA gaps, attributed to defects in Okazaki fragment processing or gap repair mechanisms (21,26,33–36). More recently, we participated in a study that showed that the BRCA1/BARD1 ubiquitin ligase ubiquitinates PCNA to promote continuous DNA synthesis, avoiding the generation of ssDNA gaps (37). In addition, treatment with PARP inhibitors (PARPi), a common therapy for homologous recombination (HR)-deficient tumors, leads to the formation of ssDNA gaps in BRCA1-deficient cells, while the emergence of PARPi resistance appears to correlate with the suppression of these gaps (26,38). Hence, targeting the formation and/or repair of ssDNA gaps could hold significant potential to maximize the efficacy of genotoxic chemotherapy.

Here, we provide evidence that ssDNA gaps readily emerge upon replication stress in wild-type human cells induced by the alkylating agent MMS or the replication inhibitor HU. These gaps are initiated by PrimPol-mediated repriming and subsequently expanded by the exonuclease EXO1, as well as the nuclease/helicase DNA2, thereby facilitating proper damage signaling through ATR activation. Interestingly, we found that EXO1 and DNA2 are essential in BRCA1-deficient cells, but not in BRCA2-deficient cells. Our data suggest a model in which the concerted actions of BRCA1, EXO1 and DNA2 in ssDNA gap expansion facilitates gap repair by TS, thereby supporting cell survival. Hence, our findings open the possibility to target EXO1 or DNA2 as a therapeutic approach to treat BRCA1-deficient tumors.

Materials and methods

Cell lines and growth conditions

RPE1 h-TERT cells were grown in high-glucose DMEM/F-12 medium with L-glutamine (Sigma-Aldrich) supplemented with 10% fetal bovine serum (Sigma-Aldrich), 100 units/ml penicillin and 100 μg/ml streptomycin (Sigma-Aldrich). RPE1 cells stably expressing YFP, YFP-EXO1 or YFP-*exo1-PIP* plasmids were grown in standard RPE1 medium supplemented with 0.5 mg/ml G418 (Gibco).

BJ-5ta, U2OS and HeLa cells were grown in high-glucose DMEM medium with L-glutamine (Sigma Aldrich) supplemented with 10% fetal bovine serum (Sigma-Aldrich), 100 units/ml penicillin, and 100 μg/ml streptomycin (Sigma-Aldrich).

MDA-MB-231, MDA-MB-436, DLD-1 and DLD-1 *BRCA2*$^{-/-}$ cells were grown in RPMI-1640 without L-glutamine (Sigma-Aldrich), supplemented with L-glutamine (Gibco), 10% fetal bovine serum (Sigma-Aldrich) 100 units/ml penicillin, and 100 μg/ml streptomycin (Sigma-Aldrich).

All cells were maintained at 37°C in 5% CO_2. Cells were regularly tested for mycoplasma contamination.

Drugs

The following drugs were used: hydroxyurea (USBiological, H9120), methyl methanesulfonate (Sigma, 129925),

4-nitroquinoline 1-oxide (Sigma, N8141), camptothecin (Sigma, C9911), DNA2 inhibitor C5 (MedChemExpress, HY-128729), MRE11 inhibitor mirin (Sigma, M9948), JH-RE-06 (Selleckchem, S8850). Concentration and duration of treatment are indicated in the corresponding figures and sections.

siRNAs, plasmids and transfections

siRNAduplexes were obtained from Sigma-Aldrich or Dharmacon (Supplementary Table S1) and were transfected using RNAiMax Lipofectamine Reagent Mix (Life Technologies), according to the manufacturer's instructions.

YFP-EXO1 plasmid was a gift from Lene J. Rasmussen (University of Copenhagen) (39). YFP-*exo1-PIP* and YFP-*exo1-D173A* mutant plasmids were generated using the QuickChange Lightening Site-Directed Mutagenesis kit (Agilent Technologies) according to the manufacture's guidelines. For the YFP-*exo1-PIP* plasmid, the previously published PIP box on EXO1 was mutated (40). Plasmid pEYFP-N1 (Clontech) was used as control. Plasmid transfections were carried out using FuGENE 6 Transfection Reagent (Promega) according to the manufacturer's protocol.

Generation of EXO1 KO cell line

For the generation of EXO1 KO cell line, Alt-R CRISPR-Cas 9 crRNA targeting the genomic sequence 5′-GCGTGGGATTGGATTAGCAA located in exon 8 of the EXO1 gene was used (ID: Hs.Cas9.EXO1.1.AA, IDT). This crRNA was duplexed with Alt-R CRISPR-Cas9 tracrRNA and transfected along with the Alt-R S.p. Cas9 nuclease V3 into RPE1 h-TERT cells following IDT guidelines. After 24 hours, transfected cells were seeded at low confluency to allow single-clone colony formation. Isolated colonies were tested for EXO1 expression by western blot. To test putative EXO1 KO clones, the CRISPR/Cas9 target site was amplified with specific primers hEXO1 CRISPR test AA down (5′ TCAAGCTCGGCTAGGAATGT) and hEXO1 CRISPR test AA up (5′ CTGCCGGGACTCAAAAAGT) and sequenced.

Chromatin fractionation

Cells were harvested and resuspended in 180 µl of Cell fractionation buffer A (10 mM HEPES pH 7.5, 10 mM KCl, 1.5 mM $MgCl_2$, 0.34 M sucrose, 10% glycerol, 1 mM dithiothreitol (DTT), complemented with 1× protease inhibitor cocktail (Roche)) + 0.1% Triton X-100, followed by incubation on ice for 15 min. At this point, a fraction of the volume was collected as whole cell extract (WCE), while the remaining volume was centrifuged at 1300g for 5 min at 4°C to precipitate the nuclei. The pellet was washed with buffer A and gently resuspended in 180 µl of Cell fractionation buffer B (20 mM HEPES pH 7.5, 3 mM EDTA, 10% glycerol, 125 mM potassium acetate, 1.5 mM $MgCl_2$, 1 mM DTT, 0.5% Triton X-100, complemented with 1× protease inhibitor cocktail) followed by incubation on ice for 30 min and centrifugation at 1700g for 5 min at 4°C to precipitate the chromatin. The pellet was washed once with buffer B, resuspended in 1× Laemmli sample buffer, and boiled at 100°C for 5 min (Chromatin sample). WCE and chromatin samples were subjected to western blotting analysis.

Western blotting

Cells were collected by scrapping in Laemmli buffer 2× (4% SDS, 20% glycerol, 125 mM Tris–HCl, pH 6.8) and boiled for 5 min at 100°C. 4× Laemmli sample buffer with β-mercaptoethanol was added to the lysates, followed by denaturation at 100°C for 5 min. Proteins were then resolved by SDS-PAGE and transferred to an Amersham Protran nitrocellulose membrane (Cytvia Life Sciences). Following incubation for 1h in blocking buffer (3–5% milk in TBS + 0.1% Tween-20), membranes were incubated with the primary antibodies diluted in blocking buffer overnight at 4°C. Anti-CHK1-pS345 (Cell Signaling #2348), anti-CHK1 (Santa Cruz #8408) anti-EXO1 (GeneTex #109 891), anti-β-Actin (Abcam #8227), anti-α-Tubulin (Sigma #T9026), anti-Vinculin (Sigma #V9131), anti-RPA2-pS4/pS8 (Bethyl #A300-245A), anti-RPA2 (Abcam #2175), anti-KAP1-pS824 (Bethyl #A300-767A), anti- γ-H2AX (Cell Signaling #2577), anti-MRE11 (Novus Biological #NB100-142), anti-PrimPol (18), anti-H3 (Abcam #1791), anti-BRCA1 (Santa Cruz #6954) and anti-BRCA2 (Millipore #OP95) primary antibodies were used. Membranes were then incubated with the appropriate infrared dyed (LI-COR) or HRP-labelled secondary antibodies and scanned in an Odyssey Infra-red Imaging System (LI-COR) or a Chemidoc MP imaging system (BioRad). Images were analyzed and quantified with ImageStudio software (LI-COR).

S1 nuclease assay

Cells were pulse-labeled with 20 µM IdU (20 min), washed twice with PBS and pulse-labeled with 200 µM CldU in the absence or presence of 1 mM MMS for 1h. Cells were then washed twice with PBS and permeabilized with CSK buffer (100 mM NaCl, 10 mM MOPS pH 7, 3 mM $MgCl_2$, 300 mM sucrose and 0.5% Triton X-100 in water) for 8 min at RT. Permeabilized cells were treated with S1 nuclease buffer (30 mM Sodium acetate pH 4.6, 10 mM zinc acetate, 5% glycerol, 50 mM NaCl in water) with or without 20 U/ml S1 nuclease (Invitrogen, 18001–016) for 30 min at 37°C. Cells were then scrapped in PBS + 0.1% BSA, pelleted and resuspended in PBS + 0.1% BSA at a final concentration of 1–2 × 10^3 cells/µl. 2.5 µl of cell suspension were spotted on a positively charged slide and lysed with 7.5 µl of spreading buffer (200 mM Tris–HCl pH 7.5, 50 mM EDTA, 0.5% SDS). After 8 min, slides were tilted at 45° to allow the DNA to spread. Slides were then air-dried, fixed with ice-cold methanol/acetic acid (3:1) for 5 mins, air-dried and stored at 4°C. Slides were rehydrated with PBS, denatured with 2.5 M HCl for 1h, washed with PBS twice, and blocked with blocking buffer (3% BSA, 0.1% Triton X-100 in PBS) for 40 min. Next, slides were incubated with primary antibody mix of mouse anti-BrdU which recognizes IdU (Becton Dickinson #347 580, 1:250) and rat anti-BrdU which recognizes CldU (Abcam #6326, 1:250) diluted in blocking buffer for 2.5 h at RT in a dark humid chamber. Slides were washed 3 times with PBS for 5 min each and incubated with secondary antibodies anti-mouse Alexa Fluor 594 and anti-rat Alexa Fluor 488 (1:250, Invitrogen #A11032 and #A11006, respectively) in blocking buffer for 1h at RT in a dark humid chamber. After washing 3 times with PBS and air-drying, slides were mounted with Prolong gold antifade reagent (Invitrogen, P36930) and stored at 4°C until imaging. Images were acquired using a AF6000 Leica Fluorescence microscope equipped with a HCX PL APO 63× (NA = 1.4) oil

objective. Fibers were measured using the segmented line tool on ImageJ FIJI software (https://fiji.sc).

Cell viability assays

Cells were seeded in 6-well plates at appropriate dilutions in triplicates. After 7–14 days, colonies were stained with a solution containing 0.5% crystal violet and 20% ethanol, followed by several washes with water. Plates were scanned with an Epson Perfection 4490 scanner and the area of the wells covered with cells was calculated using the ImageJ plugin ColonyArea (41). For viability assays upon drug treatment, 24 h after seeding, the cells were treated with DMSO as control, or with the chemical agent described in the text at the indicated concentrations. After 7–14 days, colonies were stained, scanned, and quantified as indicated previously. For the clonogenic survival shown in Figure 5C, the number of colonies were counted manually. Data are representative of at least three independent experiments.

Immunofluorescence

For RPA signal visualization, cells were seeded on coverslips. After 1 h of MMS treatment (2mM), cells were treated with pre-extraction buffer (25 mM Tris–HCl, pH 7.5, 50 mM NaCl, 1 mM EDTA, 3 mM $MgCl_2$, 300 mM sucrose and 0.2% Triton X-100) for 5 min on ice to pre-extract soluble proteins. Cells were then fixed with 4% paraformaldehyde (w/v) in PBS for 20 min.

For 53BP1 visualization, cells were seeded on coverslips. After 1 h upon addition of the indicated concentrations of the genotoxic agents, cells were fixed with ice-cold methanol for 10 min, followed by incubation with ice-cold acetone for 30 s.

In both cases, after two washes with PBS, cells were blocked for 1 h with 5% FBS in PBS, co-stained with anti-RPA (Abcam #21 752) or anti-53BP1 (Novus Biologicals #NB100-304) primary antibodies diluted in blocking buffer for 2 h at room temperature, washed again with PBS and then co-immunostained with the secondary antibodies anti-mouse Alexa Fluor 594 (Invitrogen #A11032) for RPA or anti-rabbit Alexa Fluor 488 (Invitrogen #A11034) for 53BP1 in blocking buffer for 1 h at room temperature. Coverslips were then mounted into glass slides using Vectashield mounting medium with DAPI (Vector laboratories). Images were acquired using a AF6000 Leica Fluorescence microscope equipped with a HCX PL APO 63× (NA = 1.4) oil objective. RPA signal intensities were quantified using ImageJ FIJI software.

Flow cytometry-based immunofluorescence

Cells were collected by trypsinization and treated with 4% formaldehyde (w/v) for 15 min at room temperature. After washing with PBS, cells were pelleted by centrifugation, resuspended in ice-cold methanol, and incubated for 10 min on ice. Cells were then washed with PBS and incubated with anti-CHK1-pS345 in antibody dilution buffer (0.5% BSA in PBS) for 1.5 h. Following a wash with PBS, cells were co-immunostained with the secondary antibody anti-rabbit Alexa Fluor 488 (Invitrogen #A11034) in antibody dilution buffer for 45 min at room temperature, washed with PBS and incubated with 250 μg/ml RNase A (Sigma) and 1 μg/ml DAPI (Sigma) overnight. Samples were analyzed with a LSRFortessa X-20 machine (BD Biosciences). The histograms shown in Supplementary Figure S2G were generated by gating the cell population in S-phase based on the DNA content.

Gene expression correlation and survival analysis

Correlations between the gene expressions of *BRCA1/2*, *EXO1*, *DNA2*, *BLM* and *MRE11* from the TCGA Breast Cancer (BRCA) dataset were obtained using the UCSC Xena platform (42), and plotted using PRISM software (Graphpad Software). For the survival data in Figure 6G, a correlation between *BRCA1*, *EXO1* and 'days_to_death' from the TCGA BRCA dataset was obtained from UCSC Xena web tool. After excluding the top 80% of samples with the highest *BRCA1* expression levels, the remaining samples were stratified into two groups based on *EXO1* expression levels: high (Log_2[normalized_counts + 1] above 4.5) and low (Log_2[normalized_counts + 1] below 4.5). Finally, survival data of these two groups were plotted accordingly using PRISM software.

The comparison of *EXO1* expression levels between tumor and normal samples in TCGA Breast Cancer and GTEx datasets shown in Supplementary Figure S6E was retrieved from the GEPIA platform (43), by using the Expression DIY tab, employing default fold-change and *P*-value cutoffs.

Cell cycle analysis

Cells were fixed with cold 70% ethanol overnight, incubated with 250 μg/ml RNase A (Sigma) and 10 μg/ml propidium iodide (Fluka) in PBS at 37°C for 30 min and analyzed with a FACSCalibur or a LSRFortessa X-20 machines (BD Biosciences).

Statistical analysis

Statistical significance was determined with the test indicated in the corresponding figure legend using PRISM software (Graphpad Software). Statistically significant differences were labeled with one, two, three or four asterisks if $P < 0.05$, $P < 0.01$, $P < 0.001$ or $P < 0.0001$, respectively. Specific replicate numbers (n) for each experiment can be found in the corresponding figure legends.

Results

Unreplicated ssDNA gaps are formed in response to replication stress, triggering ATR activation

The equilibrium between different DDT pathways is still poorly understood. In several studies, it has been demonstrated that PrimPol repriming is selectively activated upon cisplatin or low doses of HU, under specific conditions such as impaired fork reversal, PrimPol overexpression or BRCA deficiency (8,24,27,32,33). However, the relevance of repriming in WT cells is less understood. We then decided to use non-transformed RPE1-hTERT cells (referred to as WT in this manuscript) to investigate whether repriming plays a role in the DNA replication stress response triggered by the alkylating agent methyl methanesulfonate (MMS). First, we exposed WT cells to MMS for 1 hour, and examined the recruitment of PrimPol to chromatin. We also exposed the cells to the replication inhibitor hydroxyurea (HU), which has been shown previously to increase the amount of PrimPol on chromatin (18). Notably, both MMS and HU resulted in the accumulation of PrimPol protein on the chromatin fraction (Figure 1A). This recruitment to chromatin was further validated in BJ-5ta cells, an additional non-transformed cell line (Supplementary Figure S1).

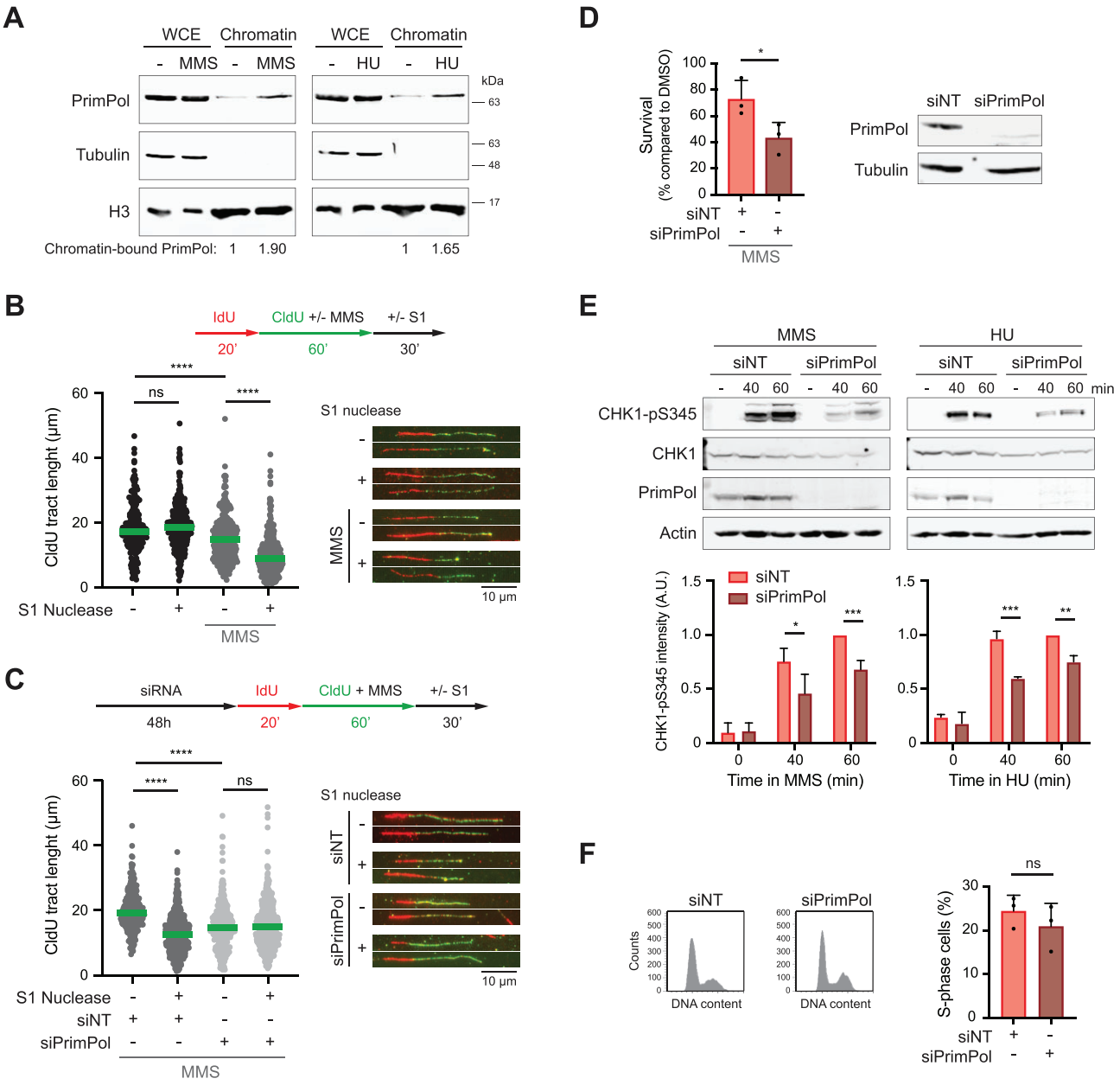

Figure 1. Unreplicated ssDNA gaps emerge as a response to replication stress, triggering ATR activation. (**A**) Immunoblots show the levels of the indicated proteins in whole cell extracts (WCE) and chromatin-enriched fractions upon treatment with MMS (left, 2 mM) or HU (right, 2 mM) for 1h. Quantification of chromatin-bound PrimPol relative to histone H3 is shown on the bottom. (**B** and **C**) Top: Scheme of the IdU/CldU pulse-labelling protocol, followed by S1 nuclease treatment. Bottom: CldU tact lengths in the indicated experimental conditions with or without S1 nuclease treatment. Each dot represents one fiber and the green bar represents the median. At least 200 fibers were measured from two biological experiments ($n = 2$). *P* values were calculated using the Mann–Whitney test (ns: $P > 0.05$; $^{****}P < 0.0001$). Representative images of DNA fibers are shown. (**D**) Viability of RPE1 cells after transfection with the indicated siRNAs, upon treatment with 0.02 mM MMS, relative to control DMSO-treated cells. Bars represent the means ± SD of independent biological replicates ($n = 3$). Values of individual experiments are indicated as dots. p values were calculated using the Student's *t*-test ($^{*}P < 0.05$). Right: Western blot for monitoring PrimPol levels 48h after transfection with control (siNT) or PrimPol siRNA. Tubulin served as loading control. (**E**) Western blots for monitoring CHK1-S345 phosphorylation in WT (RPE1) cells treated with siNT or siPrimPol, upon the addition of MMS (left, 2 mM) or HU (right, 2 mM). Actin served as loading control. Quantifications of CHK1-pS345 intensities, normalized to actin, are shown below. Bars represent the means ± SD of independent biological replicates ($n = 3$). *P*-values were calculated using the Student's *t*-test ($^{*}P < 0.05$; $^{**}P < 0.01$; $^{***}P < 0.001$). (**F**) Cell cycle profiles of siNT and siPrimPol-treated cells. Quantification of the percentage of cells in S-phase is shown on the right. Bars represent the means ± SD of independent biological replicates ($n = 3$). Values of individual experiments are indicated as dots. p values were calculated using the Student's *t*-test (ns: $P > 0.05$).

To precisely assess whether ssDNA gaps were generated in response to MMS, we used the S1 nuclease DNA fiber method (44). In this assay, after consecutive pulse-labelling with two thymidine analogs, IdU and CldU, cells are permeabilized and incubated with the S1 endonuclease that specifically cleaves ssDNA. This treatment shortens the DNA tracts if gaps are present in nascent DNA. Control samples showed that the CldU tract length remained unchanged upon S1 digestion. However, when MMS was added during the CldU labelling, the tracts became sensitive to S1 nuclease (Figure 1B), thereby indicating the formation of gaps within the DNA strands. Accordingly, depletion of PrimPol prevented the CldU tracts from shortening after S1 treatment (Figure 1C). Notably, in the absence of S1 nuclease treatment, CldU tracts were shorter in PrimPol-depleted cells compared to control cells (Figure 1C), suggesting a role of PrimPol during replication through MMS-induced lesions. In line with this observation, loss of PrimPol sensitized human RPE1 cells to MMS exposure (Figure 1D), consistent with previous findings in avian cells (45). Taken together, these data indicate that ssDNA gaps are readily generated upon MMS treatment through repriming by PrimPol. Interestingly, HU treatment has also been demonstrated to result in accumulation of ssDNA gaps in budding yeast, as well as in BRCA1/2-deficient human cells (32,46). Therefore, our findings, along with those of others, suggest that the formation of ssDNA gaps via PrimPol repriming activity is a common response to any form of replication stress even in wild-type human cells.

The general concept derived from previous studies postulates that during replication stress, checkpoint kinases are activated by regions of ssDNA arising at stalled forks (47,48). If this is the case, effective repriming would prevent the accumulation of ssDNA at forks, thereby precluding the full activation of the replication checkpoint. To examine this hypothesis, we analyzed the phosphorylation of CHK1 at Ser^{345}, as a readout of ATR activation, at very early timepoints after the addition of MMS or HU in the absence of PrimPol (Figure 1E). Intriguingly, depletion of PrimPol led to a notable decrease in the phosphorylation of CHK1 after both treatments. It is important to note that a decline in CHK1 phosphorylation could be explained by a reduction in the number of cells in S-phase. However, we observed only a marginal, statistically non-significant decrease in the proportion of cells in S-phase in the absence of PrimPol compared to control that cannot account for the pronounced differences observed in ATR activation (Figure 1F). Taken together, our results suggest that the signal triggering ATR activation in response to replications stress mainly originates from PrimPol-dependent post-replicative ssDNA gaps in wild-type human cells.

EXO1 activity is required for robust ATR activation

In budding yeast, post-replicative ssDNA gaps need to be enlarged by various factors, including the exonuclease Exo1, in order to generate an adequate checkpoint signal (31). Based on our observations that ssDNA gaps are generated in human cells in response to replication stress, we wonder whether EXO1-mediated gap expansion may also be a pre-requisite for producing a sufficient checkpoint signaling. To address this question, we generated a CRISPR/Cas9-mediated EXO1 KO cell line in RPE1-hTERT cells (referred to as *exo1* in this manuscript). We initially monitored the accumulation of ssDNA in both WT and *exo1* cells, using as a readout the signal intensity of the ssDNA-binding protein RPA within the nucleus, detected by immunofluorescence (Figure 2A). Notably, RPA mean intensity in RPA-positive cells, which correspond to those in S-phase, was highly increased in the WT after MMS treatment. However, in cells lacking EXO1, such increased in RPA intensity was significantly lower. Thus, this data suggests that EXO1 activity promotes the accumulation of ssDNA in the presence of damaged DNA.

Next, we evaluated whether a reduction in the overall accumulation of ssDNA could potentially have an impact on the activation of the ATR checkpoint. We then analyzed the phosphorylation of CHK1 at Ser^{345} at very early timepoints upon addition of MMS, HU or 4-Nitroquinoline 1-oxide (4-NQO), an ultraviolet radiation-mimetic compound (Figure 2B and Supplementary Figure S2A). Indeed, the phosphorylation of CHK1 was significantly delayed in *exo1* when compared to wild-type cells following all the treatments. However, the observed difference was no longer evident after extending the treatment for up to three hours, during which the signal reached saturation (Supplementary Figure S2B). This indicates that the requirement of EXO1 for the full activation of ATR depends on the extent of the damage. Additionally, the defect in ATR activation was further validated in a second KO clone of EXO1 in RPE1 cells, as well as in the non-cancer cell line BJ-5ta and the cancer cell lines U2OS and HeLa by siRNA-mediated depletion of EXO1 (Supplementary Figure S2C-F). Notably, no significant changes were observed in the cell cycle profiles of EXO1-lacking cells compared to control (Figure 2C and Supplementary Figure S2C–F). To completely rule out the possibility that the defect in CHK1 phosphorylation was due to a reduction in the number of cells in S-phase, we monitored the intensity of CHK1 phosphorylation in single cells using a flow cytometry-based immunofluorescence assay (Figure 2D and Supplementary Figure S2G). After subjecting WT cells to HU or MMS treatments, we found a noticeable increase in CHK1-pS345 intensity from the background levels shown in untreated cells. This increase was particularly evident in the fraction of cells in S-phase. However, in *exo1* cells, this increase was relatively lower, which further support the idea that EXO1 is required for timely and robust ATR activation upon induction of replication stress in human cells. Additionally, we observed that CHK1 phosphorylation upon HU treatment became EXO1-independent when repriming was prevented through PrimPol depletion (Figure 2E), suggesting a role of EXO1 in promoting ATR activation through the expansion of post-replicative ssDNA gaps.

EXO1 is involved in long-range resection during the homologous recombination pathway for double-strand break (DSB) repair, thus generating ssDNA from the DNA ends that activates the ATR checkpoint (49). Therefore, the observed delay in ATR activation in *exo1* cells could be attributed to an impairment in DNA-end resection following the potential formation of DSBs by the treatments with the different genotoxic agents. We then set to look for evidence of DSB formation under the moderate damage conditions used in this study. First, we conducted western blot experiments to examine the phosphorylation RPA2 at S4/S8 and KAP1 at S824 (Supplementary Figure S3A). These phosphorylation events serve as indicators of ATM/DNA-PK activation and are commonly used as markers for DSBs (20). The topoisomerase I inhibitor camptothecin (CPT) was used as positive control for DSBs formation (50). Treatments for up to 1h with the selected doses of MMS, HU and 4-NQO did not reveal any

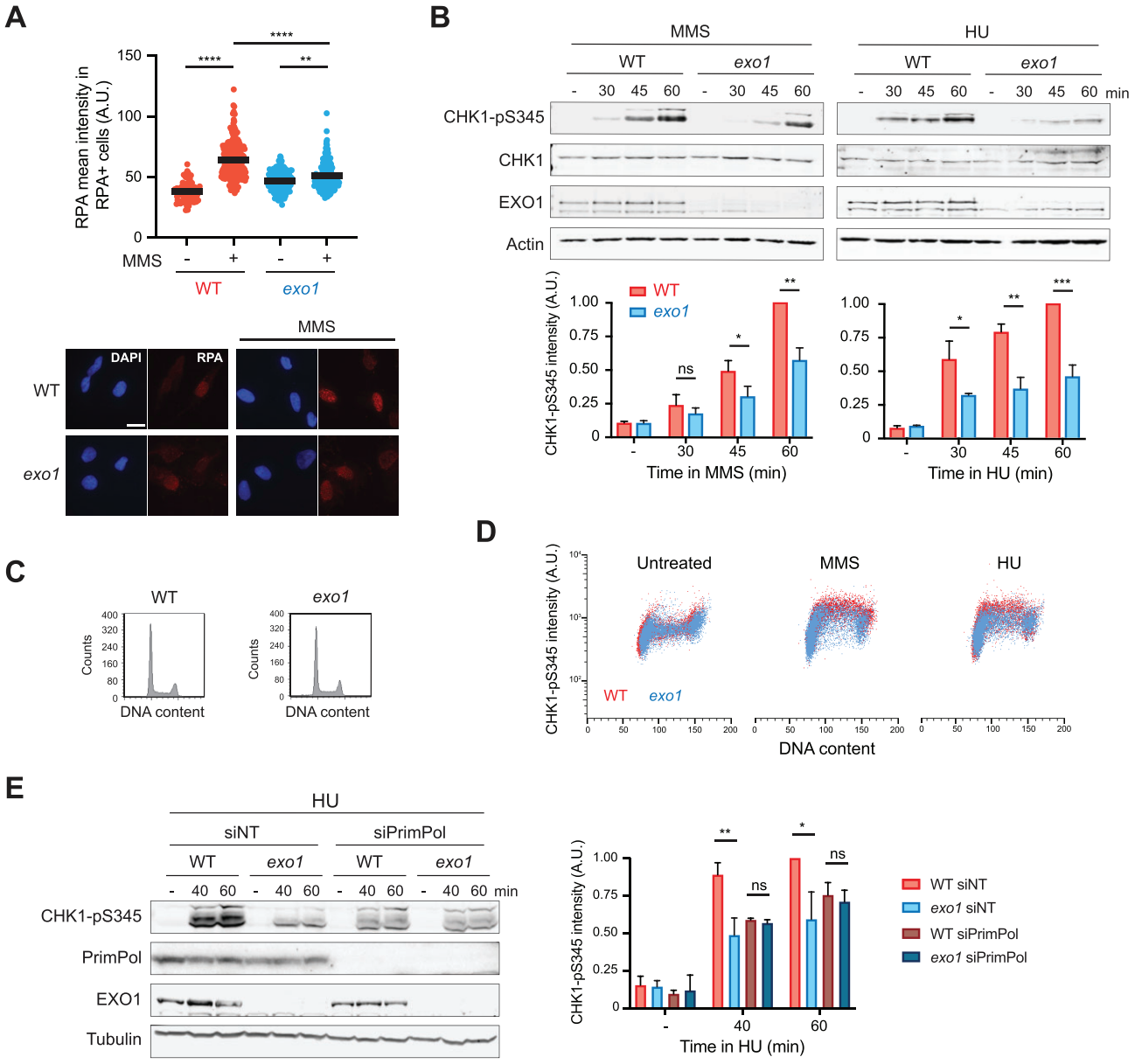

Figure 2. EXO1 function is required for ssDNA accumulation and, consequently, robust ATR checkpoint activation upon replicative stress. (**A**) Quantification of the RPA mean signal intensity in the fraction of cells positive for RPA in WT and *exo1* cells treated with or without MMS (2 mM) for 1 h. Each dot represents the RPA mean intensity inside the nucleus and the black bar represents the mean. Bottom: representative images. Scale bar, 20 μm. (**B**) Western blots for monitoring CHK1-S345 phosphorylation in WT and *exo1* cells upon addition of MMS (left, 2 mM) or HU (right, 2 mM). Actin served as loading control. Quantifications of CHK1-pS345 intensities, normalized to actin, are shown below. Bars represent the means ± SD of independent biological replicates ($n = 3$). *P*-values were calculated using the Student's *t*-test (ns: $P > 0.05$; $^{*}P < 0.05$; $^{**}P < 0.01$; $^{***}P < 0.001$). (**C**) Cell cycle profiles of WT and *exo1* cells. (**D**) Quantifications of CHK1-pS345 signal intensities in WT (red) and *exo1* (blue) cells by flow cytometry-based immunofluorescence, left untreated or treated with MMS (2 mM) or HU (2 mM) for 1h. Each dot represents a single cell. 10 000 cells are displayed per condition. (**E**) Western blots for monitoring CHK1-S345 phosphorylation in WT and *exo1* cells treated with siNT or siPrimPol, upon the addition of HU (2mM). Tubulin served as loading control. Quantification of CHK1-pS345 intensities, normalized to tubulin, is shown on the right. Bars represent the means ± SD of independent biological replicates (n = 3). *P*-values were calculated using the Student's *t*-test (ns: $P > 0.05$; $^{*}P < 0.05$; $^{**}P < 0.01$).

significant increase in the phosphorylation levels of RPA2. However, a slight increase in phospho-KAP1 was detected after 1h, specially upon MMS, albeit considerably lower than the substantial increase observed upon treatment with CPT (Supplementary Figure S3A). MMS and HU have been already shown to induce phosphorylation of KAP1 without detectable DSB formation and RPA2 S4/S8 phosphorylation, supporting the notion of DSB-independent activation of ATM by replication stress (20). Intriguingly, ATR activation, as detected by phosphorylation of CHK1, was similar following all the treatments, thus supporting the idea that ATR was activated by different structures (Supplementary Figure S3A). Second, we analyzed the formation of 53BP1 foci, as a marker for the non-homologous end-joining (NHEJ) pathway for DSB repair (Supplementary Figure S3B). In agreement with the western blot data, 53BP1 foci were detected 1h after the addition of CPT but not MMS, HU or 4-NQO. Collectively, these findings suggest that EXO1 facilitates ATR activation through the pro-

cessing of structures other than DSBs, likely involving post-replicative ssDNA gaps.

Robust ATR activation requires both the capacity of EXO1 to bind PCNA and its nuclease activity

EXO1 has been shown to interact with PCNA through a PCNA-interacting Protein region (PIP-Box)-like sequence located at the C-terminus of the protein (39). This interaction has been shown to promote EXO1 damage recruitment and processivity during DSB repair (40). We then sought to elucidate if the interaction of EXO1 with PCNA was required for ATR checkpoint activation upon induction of replicative stress. To do so, we generated stable cell lines expressing an empty vector, a YFP-tagged wild-type version of EXO1 gene (YFP-EXO1) or a YFP-tagged PIP box mutant of EXO1 (YFP-*exo1-PIP*) and monitored the activation of ATR upon MMS treatment by the phosphorylation of CHK1 (Figure 3A–C). Accordingly, when compared to the WT, ATR activation was delayed in *exo1* cells expressing an empty vector, and this defect was nearly completely rescued in *exo1* cells expressing the wild-type EXO1 gene (Figure 3A, B). However, despite retaining its nuclease activity (40), the PIP-box mutant of EXO1 failed to rescue this delay (Figure 3C), thus indicating that an interaction of EXO1 with PCNA is required for efficient ATR activation.

EXO1 encodes both structural and catalytic functions, each playing distinct roles in DNA metabolic pathways (51). To discern which function of EXO1 is crucial for ATR activation, we analyzed the phosphorylation of CHK1 in *exo1* cells expressing the nuclease-dead *exo1-D173A* mutant (Figure 3D). As expected, the expression of *exo1-D173A* also failed to restore the delay in CHK1 phosphorylation observed in *exo1* cells expressing an empty vector. Hence, this data indicates that the catalytic activity of EXO1 is essential for promoting robust ATR activation,

DNA2, but not MRE11, activity is required for ATR activation

Next, we investigated whether the complete activation of ATR requires the involvement of other nucleases in addition to EXO1. First, we examined the role of MRE11, a component of the MRE11-RAD50-NBS1 (MRN) complex responsible for recognizing DSBs and initiating DNA-end resection (49,52). Interestingly, MRE11 has also been implicated in the resection of ssDNA gaps, thereby facilitating RAD51 loading and subsequent homologous recombination (HR)-dependent repair of the gaps (23,53). However, the depletion of MRE11 had no discernable impact on either the phosphorylation levels of CHK1 following MMS treatment or the cell cycle profile, when compared to the control samples (Supplementary Figure S4A and B). Additionally, the inhibition of the exonuclease activity of MRE11 by mirin did not produce any noticeable impact on phospho-CHK1 levels following MMS exposure (Supplementary Figure S4C).

Then, we focused on DNA2, a nuclease/helicase involved in long-range resection during the homologous recombination pathway for DSB repair (49,52). To avoid the toxicity associated with siRNA-mediated depletion of DNA2, we used the specific DNA2 inhibitor C5 (54). Interestingly, the phosphorylation of CHK1 was significantly delayed upon MMS or HU treatment when DNA2 was inhibited (Figure 4A). Notably, the cell cycle profile of DNA2-inhibited cells remained similar to that of the control cells (Figure 4B), thereby ruling out any cell cycle contribution to the observed phenotype. Interestingly, the delay in CHK1 phosphorylation following MMS or HU treatment was further prolonged when both EXO1 was absent and DNA2 was inhibited (Figure 4C), indicating that they likely work in alternative pathways. Taken together, our results indicate that both EXO1 and DNA2 play a pivotal role as the primary nucleases involved in the generation of the ssDNA signal that activates the ATR checkpoint upon replication stress, whereas the impact of MRE11 appears to be more restricted.

EXO1 and DNA2 expand ssDNA gaps behind the replication forks

Our observations suggest that ssDNA gaps arising behind the replication forks in cells exposed to replication stress are expanded by EXO1 and DNA2 nucleases, thereby contributing to the full activation of the ATR checkpoint in human cells. To confirm this hypothesis and obtain direct evidence of gap expansion, we initially monitored the formation of ssDNA gaps in *exo1* cells using the S1 nuclease DNA fiber assay. We reasoned that if EXO1 expands ssDNA gaps, its absence would result in an increased probability that gaps remain undigested during S1 nuclease treatment. Indeed, while DNA tracts undergo shortening in WT cells treated with MMS when subjected to S1 nuclease digestion, they became insensitive to S1 nuclease in *exo1* cells (Figure 1B and 5A). Notably, we ruled out the possibility of a repriming deficiency, since PrimPol was effectively recruited to chromatin in *exo1* cells (Supplementary Figure S5). Finally, inhibition of DNA2 also rendered DNA tracts insensitive to S1 nuclease digestion (Figure 5B). Taken together, our findings suggest that both EXO1 and DNA2 are crucial for post-replicative ssDNA gap expansion, thereby enabling ATR activation.

The expansion of ssDNA gaps has been proposed to be a prerequisite for successful template switching pathway of DNA damage tolerance (10,19,23,31,55,56). When TS is impaired, cells tend to rely more on translesion synthesis for repairing ssDNA gaps arising during DNA replication. This is the case for HR-deficient cells, such as *BRCA1/2* mutant cells, which accumulate ssDNA gaps during unperturbed DNA replication and exhibit increased toxicity to the inhibition of the REV1-Polζ-dependent TLS (33,37). We then tested the sensitivity of *exo1* cells to the REV1-Polζ inhibitor JH-RE-06 (Figure 5C). In agreement with a role of EXO1 in TS, *exo1* cells exhibited a considerably higher sensitivity to JH-RE-06 treatment compared to WT cells, resulting in a reduction of 50% in clonogenic survival. Interestingly, the sensitivity of *exo1* cells to JH-RE-06 was further enhanced when replicative stress was induced through chronic MMS treatment, leading to a further reduction in clonogenic survival when compared to WT cells (Figure 5C). Hence, these findings suggest that EXO1 plays a critical role in expanding ssDNA gaps generated during replication stress, a process essential for the subsequent repair by TS. Thus, a deficiency in TS renders *exo1* cells more reliant on TLS to deal with replication stress.

EXO1 and DNA2 functions are essential for BRCA1-deficient cells

Given that BRCA1/2 proteins promote the repair of ssDNA gaps through the TS pathway, and our data indicate that EXO1-mediated gap extension is also crucial for TS, we

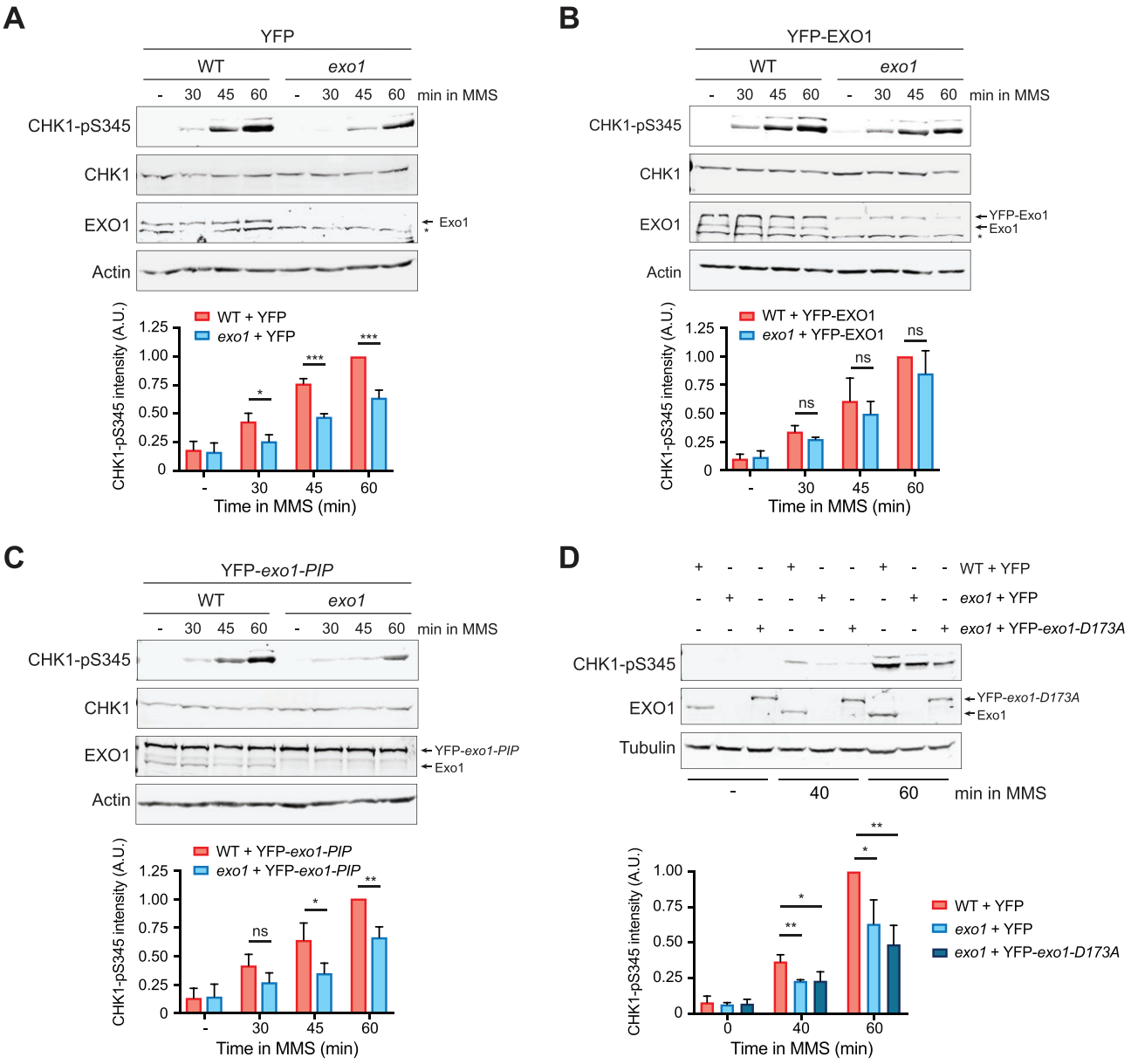

Figure 3. Robust ATR checkpoint activation upon replicative stress requires the interaction between EXO1 and PCNA, along with the catalytic activity of EXO1. Western blots for monitoring CHK1-S345 phosphorylation in WT and *exo1* cells stably expressing an empty vector (**A**) a YFP-tagged EXO1 (**B**) and a YFP-tagged *exo1* PIP-box mutant (**C**) upon addition of MMS (2 mM). Actin served as loading control. Quantifications of CHK1-pS345 intensities, normalized to actin, are shown below. Bars represent the means ± SD of independent biological replicates (n = 3). *P*-values were calculated using the Student's *t*-test (ns: $P > 0.05$; $^{*}P < 0.05$; $^{**}P < 0.01$; $^{***}P < 0.001$). (**D**) Western blots for monitoring CHK1-S345 phosphorylation in WT and *exo1* cells stably expressing an empty vector, and *exo1* cells transiently expressing a YFP-tagged *exo1-D173A* mutant, upon addition of MMS (2 mM). Tubulin served as loading control. Quantifications of CHK1-pS345 intensities, normalized to tubulin, are shown below. Bars represent the means ± SD of independent biological replicates ($n = 3$). *P*-values were calculated using the Student's *t*-test (ns: $P > 0.05$; $^{*}P < 0.05$; $^{**}P < 0.01$).

set to investigate the potential repercussions of EXO1 loss in *BRCA1/2* mutant background. Strikingly, depletion of EXO1 significantly reduced the viability of a BRCA1-deficient breast cancer cell line (MDA-MB-436) but had no effect on a BRCA1-proficient breast cancer cell line (MDA-MB-231) (Figure 6A and Supplementary Figure S6A). This reduction in the viability of BRCA1 and EXO1-deficient cells was further validated in RPE1 and U2OS cell lines (Supplementary Figure S6B and C). Interestingly, this phenotype was specific to BRCA1, as the absence of EXO1 did not impact the survival of either a BRCA2-deficient DLD1 or a BRCA2-depleted RPE1 cell line (Supplementary Figures S7A and S6B). Moreover, inhibition of mutagenic TLS by treatment with JH-RE-06 showed additive cytotoxicity when combined with the depletion of EXO1 in the BRCA1-deficient cancer cell line (Figure 6B), thus further supporting the idea that EXO1 and TLS polymerases operate in distinct, complementary, pathways.

Next, we investigated whether the observed synthetic lethality between BRCA1 and EXO1 could be associated with a combined impairment in gap extension, considering the role of BRCA1, but not BRCA2, in promoting resection (57). In line with this hypothesis, we detected a defect in CHK1

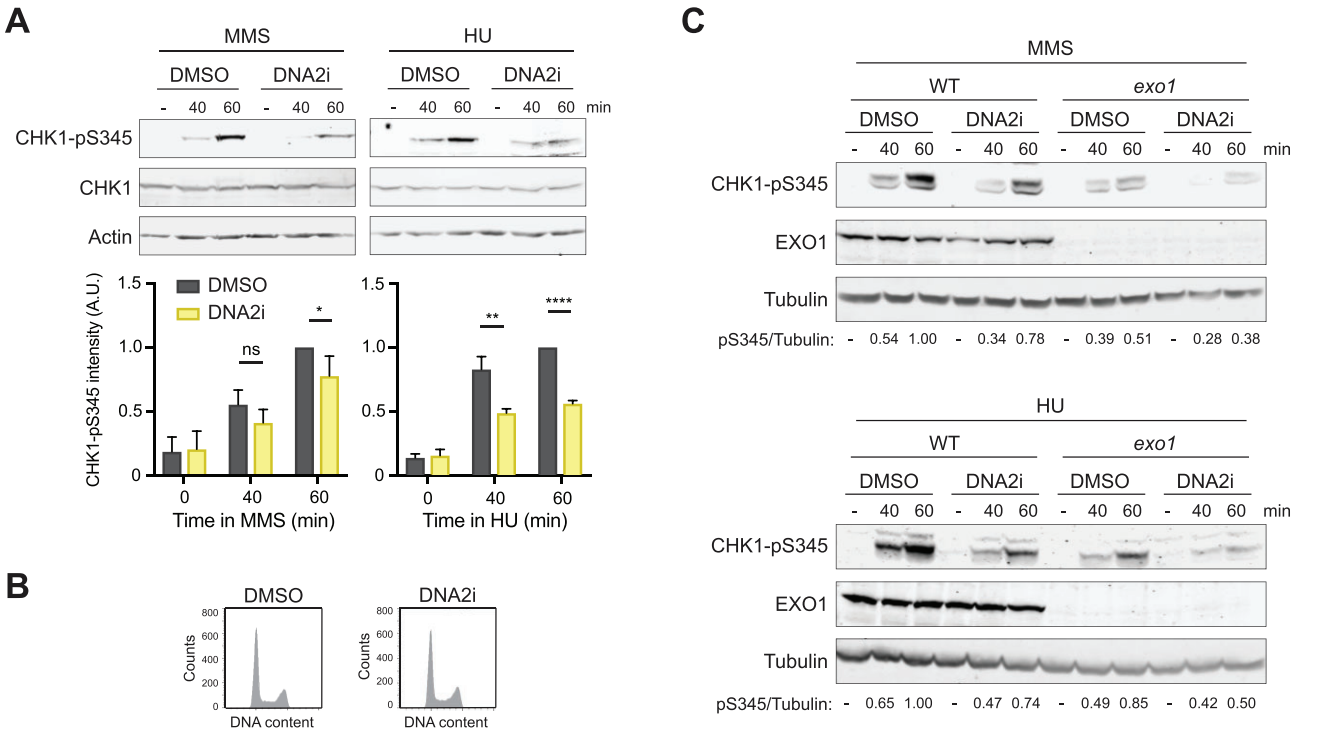

Figure 4. DNA2 activity is required for ATR checkpoint activation upon replication stress, operating as an alternative pathway to EXO1. (**A**) Western blots for monitoring CHK1-S345 phosphorylation in WT (RPE1) cells treated with DMSO or DNA2 inhibitor C5 (20 μM) for 5 h before the addition of MMS (2 mM) or HU (2 mM). Bottom panels: Quantification of CHK1-pS345 intensities, normalized to the loading control. Bars represent the means ± SD of independent biological replicates ($n = 4$ for MMS, $n = 3$ for HU). *P*-values were calculated using the Student's *t*-test (ns: $P > 0.05$; $^{*}P < 0.05$; $^{**}P < 0.01$; $^{****}P < 0.0001$). (**B**) Cell cycle profiles in control (DMSO) or DNA2i-treated cells. (**C**) Western blots for monitoring CHK1-S345 phosphorylation in WT and *exo1* cells treated with DMSO or DNA2 inhibitor C5 (20 μM) for 5 h before the addition of MMS (top, 2 mM) or HU (bottom, 2 mM). Tubulin served as loading control. Quantifications of CHK1-S345 phosphorylation relative to tubulin are shown on the bottom. The experiment was repeated at least twice, independently, with similar results.

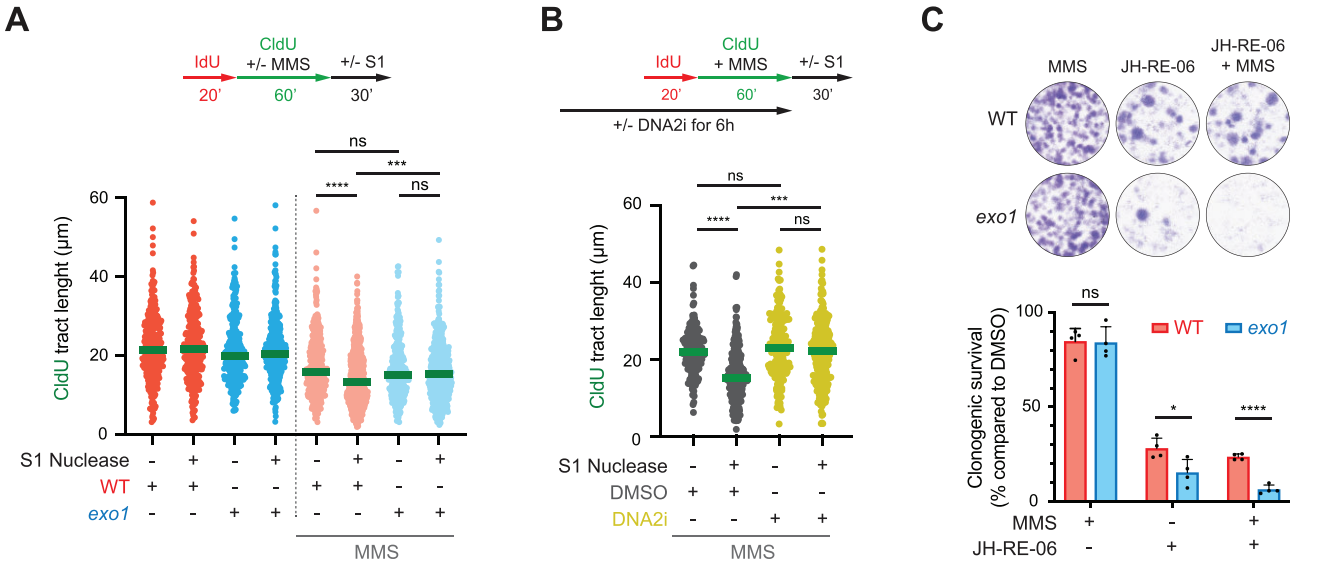

Figure 5. EXO1 and DNA2 facilitate the expansion of ssDNA gaps and EXO1 promotes cell survival upon treatment with the REV1-Polζ inhibitor JH-RE-06. (**A**) and (**B**) Top: Scheme of the IdU/CldU pulse-labelling protocol, followed by S1 nuclease treatment. Bottom: CldU tact lengths in the indicated experimental conditions with or without S1 nuclease treatment. Each dot represents one fiber and the green bar represents the median. At least 275 fibers were measured from two biological experiments ($n = 3$). *P* values were calculated using the Mann-Whitney test (ns: $P > 0.05$; $^{***}P < 0.001$; $^{****}P < 0.0001$). (**C**) Clonogenic survival of WT and *exo1* cells treated with MMS (0.05 mM) and/or JH-RE-06 (0.25 μM). Top: Representative images. Bottom: Quantification of the clonogenic survival as a percentage of the number of colonies formed relative to control DMSO-treated cells. Bars represent the means ± SD of independent biological replicates ($n = 4$). Values of individual experiments are indicated as dots. *P* values were calculated using the Student's *t*-test (ns: $P > 0.05$; $^{*}P < 0.05$; $^{****}P < 0.0001$).

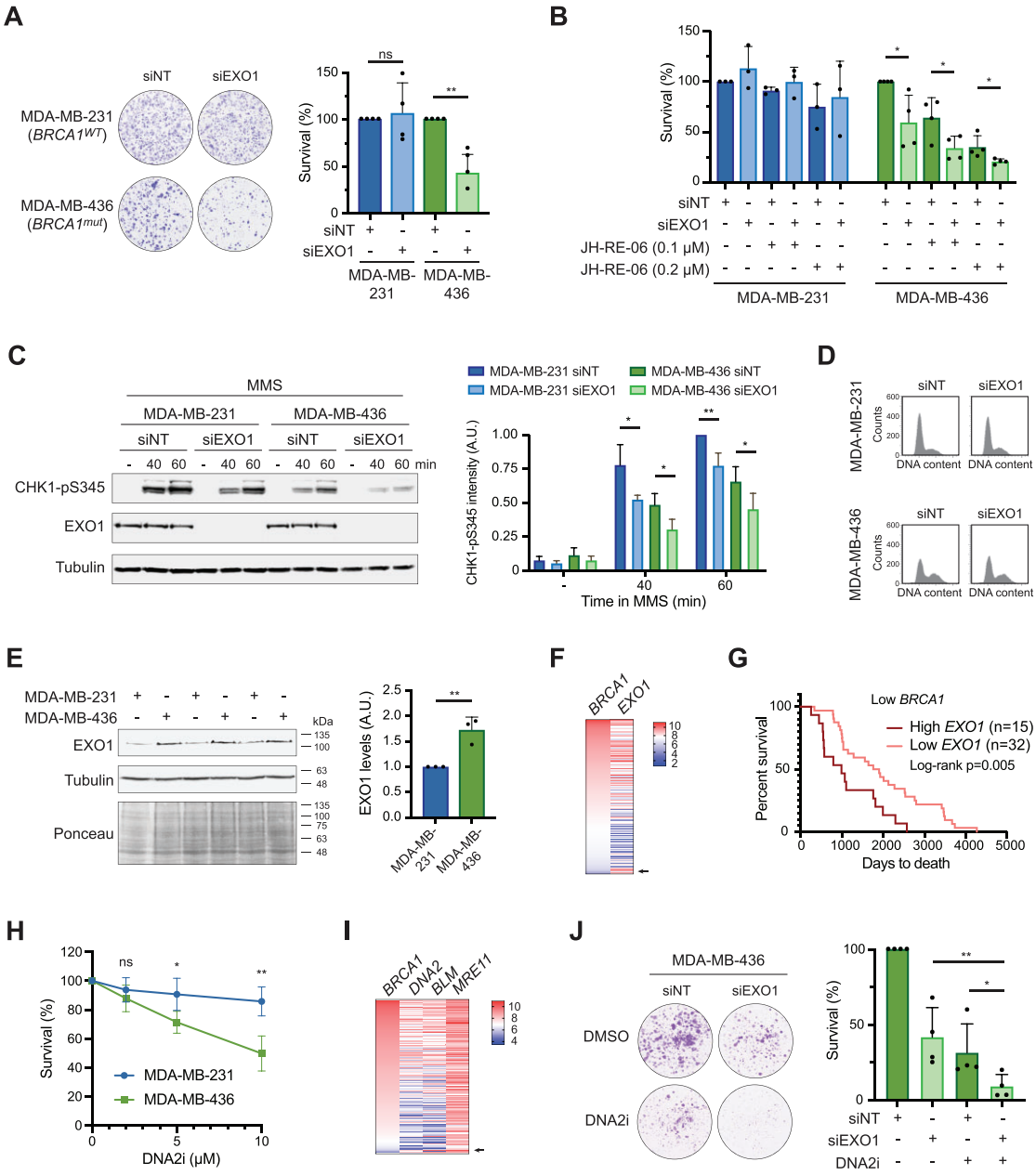

Figure 6. EXO1 and DNA2 are essential for BRCA1-mutant cells. (**A**) Viability of MDA-MB-231 (*BRCA1*^{WT}) and MDA-MB-436 (*BRCA1*^{mut}) cells after transfection with the indicated siRNAs. Left: Representative images. Right: Quantification of cell survival as percentage of viable cells relative to siRNA control. Bars represent the means ± SD of independent biological replicates ($n = 4$). Values of individual experiments are indicated as dots. p values were calculated using the Student's *t*-test (ns: $P > 0.05$; $^{**}P < 0.01$). (**B**) Viability of MDA-MB-231 and MDA-MB-436 cells after transfection with the indicated siRNAs upon treatment with JH-RE-06 at the indicated concentrations. Bars represent the means ± SD of independent biological replicates ($n = 3$ for MDA-MB-231, n = 4 for MDA-MB-436). Values of individual experiments are indicated as dots. *P* values were calculated using the Student's *t*-test (ns: $P > 0.05$; $^{*}P < 0.05$). (**C**) Western blots for monitoring CHK1-S345 phosphorylation in MDA-MB-231 and MDA-MB-436 cells treated with siNT or siEXO1, upon the addition of MMS (2 mM). Tubulin served as loading control. Quantification of CHK1-pS345 intensities, normalized to tubulin, is shown on the right. Bars represent the means ± SD of independent biological replicates ($n = 3$). *P*-values were calculated using the Student's *t*-test ($^{*}P < 0.05$; $^{**}P < 0.01$). (**D**) Cell cycle profiles in MDA-MB-231 and MDA-MB-436 cells treated with siNT or siEXO1. (**E**) Western blot showing EXO1 protein levels in MDA-MB-231 and MDA-MB-436 cells. Tubulin and Ponceau served as loading controls. Quantifications of EXO1 levels, normalized to tubulin, are shown on the right. Bars represent the means ± SD of independent biological replicates ($n = 3$). *P* value was calculated using the Student's *t*-test ($^{**}P < 0.01$). (**F**) Heat map of the correlation between *BRCA1* and *EXO1* expressions retrieved from TCGA Breast Cancer (BRCA) dataset using UCSC Xena ($n = 1218$). The arrow indicates the samples referred in the text. (**G**) Survival of breast cancer patients with low expression levels of *BRCA1*, stratified according to their *EXO1* levels in two categories: high (dark red) or low (light red). Data from TCGA BRCA dataset. The number of samples is indicated. (**H**) Viability of MDA-MB-231 and MDA-MB-436 cells treated with DMSO or the indicated concentrations of DNA2i. Data represent the means ± SD of independent biological replicates ($n = 4$). *P*-values were calculated using the Student's *t*-test (ns: $P > 0.05$; $^{*}P < 0.05$; $^{**}P < 0.01$). (**I**) Heat map of the correlation between *BRCA1*, *DNA2*, *BLM* and *MRE11* expressions retrieved from TCGA BRCA dataset using UCSC Xena ($n = 1218$). The arrow indicates the samples referred in the text. (**J**) Viability of MDA-MB-436 after transfection with siNT or siEXO1 upon treatment with DMSO or DNA2i (10 μM). Left: Representative images. Right: Quantification of cell survival as percentage of viable cells relative to siRNA control. Bars represent the means ± SD of independent biological replicates ($n = 4$). Values of individual experiments are indicated as dots. *P* values were calculated using the Student's *t*-test ($^{*}P < 0.05$; $^{**}P < 0.01$).

phosphorylation following MMS exposure in the BRCA1-deficient MDA-MB-436 cell line compared to BRCA1-proficient MDA-MB-231, which was accentuated upon depletion of EXO1 (Figure 6C), despite observing a higher proportion of S-phase cells in MDA-MB-436 compared to MDA-MB-231 (Figure 6D). This finding was further corroborated in RPE1 cells, where the depletion of BRCA1 in EXO1-lacking cells resulted in a marked delay in CHK1 phosphorylation, exceeding the impact observed in either single absence condition (Supplementary Figure S6D). Again, this observation was not evident in BRCA2-deficient DLD1 cell line (Supplementary Figure S7B). Collectively, our observations suggest that both BRCA1 and EXO1 promote ATR activation by facilitating the expansion of ssDNA gaps. Hence, a deficiency in gap processing, which is known to be crucial for effective gap filling by TS pathway, could contribute to the synthetic lethality observed in the absence of EXO1 and BRCA1.

Interestingly, EXO1 has been reported to be deregulated in several cancers (58). Indeed, data from The Cancer Genome Atlas (TCGA) shows that *EXO1* is overexpressed in breast cancer tissues compared to control (Supplementary Figure S6E). Therefore, we hypothesized that BRCA1-deficient cells might be particularly addicted to *EXO1* overexpression. In fact, we observed a significant increase in EXO1 protein levels in BRCA1-deficient compared to BRCA1-proficient cells (Figure 6E). Furthermore, through a comparison of *EXO1* and *BRCA1* mRNA expression levels from TCGA breast cancer (BRCA) dataset, we observed that breast tumor samples exhibiting extremely low expression of *BRCA1* gene tended to display an elevated expression of *EXO1* (Figure 6F, arrow). However, this link was not as prominently observed in breast cancer patients with low expression of *BRCA2* (Supplementary Figure S7C). Additionally, we observed that breast cancer patients with tumors expressing lower *BRCA1* levels had a more favorable prognosis specifically within the cohort exhibiting lower expression levels of *EXO1* (Figure 6G). Hence, our findings revealed that elevated *EXO1* expression correlates with BRCA1 deficiency and promotes tumor survival. These results open up the possibility of exploiting EXO1 inhibition in the clinic as a potential therapeutic strategy for BRCA1-deficient tumors.

Notably, these findings do not appear to be exclusive to EXO1 but are shared with DNA2 since we also found that BRCA1-deficient cells were significantly more sensitive to DNA2 inhibition than BRCA1-proficient cells (Figure 6H), a phenomenon that was not observed in BRCA2-deficient cells (Supplementary Figure S7D). In addition, we also found elevated expression of *DNA2,* and its partner during long-range resection, *BLM,* in breast tumor samples with very low *BRCA1* expression, while this phenomenon was not as evident in the case of the short-range resection factor *MRE11* (Figure 6I, arrow). Again, this link was not observed in breast cancer patients with low expression of *BRCA2* (Supplementary Figure S7E). Importantly, consistent with our observations that EXO1 and DNA2 work in alternative pathways for ssDNA gap expansion, BRCA1-deficient cells exhibit greater sensitivity when both EXO1 depletion and DNA2 inhibition were combined (Figure 6J). Collectively, these results suggest that BRCA1-deficient cancer cells, in contrast to BRCA2-deficient cells, require a hyper-activation of long-range DNA resection factors for their survival.

Discussion

While it is widely accepted that RPA-coated ssDNA is the signal that activates the ATR checkpoint upon replication stress, the exact origin of this signal remains less understood. The prevailing model posits that ssDNA accumulates at replication forks as a result of a functional uncoupling of the MCM helicase from the replicative polymerases (47). However, this model does not consider the possibility of repriming. Here, we present data supporting an alternative model whereby the activation of the ATR checkpoint upon replicative stress in human cells occurs at PrimPol-generated post-replicative ssDNA gaps, expanded by EXO1 and DNA2, rather than directly at replication forks due to helicase uncoupling (Figure 7). Intriguingly, we observed only a limited contribution of human MRE11 on checkpoint activation, which contrasts with previous studies suggesting a role of this protein in gap expansion (23,53). Thus, our observations indicate that the generation of sufficient ssDNA for ATR activation is primarily driven by factors involved in long-range resection, rather than MRE11-dependent short-range resection. However, whether EXO1 and/or DNA2 can compensate the absence of MRE11 remains to be explored. Notably, the proposed model of checkpoint activation is not limited to human cells but appears to be more general, as García-Rodríguez and colleagues previously identified processed-ssDNA gaps as the source of damage checkpoint signaling during replication in *Saccharomyces cerevisiae* (31). Furthermore, this EXO1-dependent mechanism of checkpoint amplification extends beyond post-replicative ssDNA gaps to encompass other structures, including DSBs, uncapped telomeres, or gaps arising from Nucleotide Excision Repair intermediates (59–61). Importantly, nuclease activity targeting ssDNA gaps must be carefully controlled to prevent the harmful consequences of over-resection. In this context, ATR activation has been demonstrated to initiate a negative feedback mechanism that prevents excessive resection via phosphorylation of, at least, EXO1 (31,62).

The generation of these ssDNA gaps may depend on factors such as timing, the dosage of the genotoxic agent, or the genetic background (4). We demonstrated that, in our experimental setup, gaps were generated upon exposure to MMS without a noticeable formation of DSBs. We then established a link in EXO1-lacking or DNA2-inhibited cells between the defective checkpoint activation and the extension of gap size, as we observed that DNA tracts became insensitive to S1 nuclease digestion following MMS treatment (Figure 5A and B), possibly due to ineffective digestion when gaps are shorter. As an alternative explanation, the use of DNA spreading may not facilitate the separation of sister chromatids, potentially hindering the detection of DNA tract shortening by S1 treatment unless there is an overlap of ssDNA regions in both adjacent sister chromatids, as shown in recent work from the Caldecott and Vindigni labs (63). Thus, one can hypothesize that, in the absence of EXO1 or DNA2, gaps are less likely to overlap and become undetectable by S1 treatment on DNA spreads. Remarkably, ssDNA gaps seem to form not only upon exposure to agents causing polymerase-blocking lesions but also in response to lesion-less replication stress induced by HU (4,27,46). Accordingly, we noticed that in the absence of PrimPol, ATR activation following HU occurred independently of EXO1. Yet, it remains unclear why repriming is the chosen pathway for DDT in situations where replication forks do not face DNA lesions. However, repriming may result from the

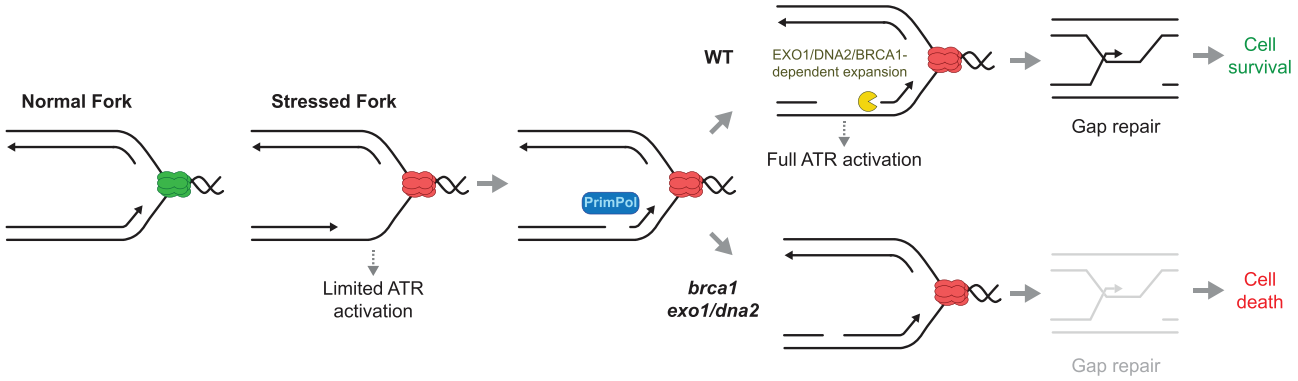

Figure 7. Schematic representation of the proposed model. Following replication stress, the emergence of PrimPol-dependent post-replicative ssDNA gaps reduces the exposure of ssDNA at the replication forks. The expansion of these gaps, facilitated by BRCA1 and the nucleases EXO1 and DNA2, not only promotes robust ATR activation but also their repair by TS, thereby supporting cell survival. When BRCA1 is absent, the accumulation of ssDNA gaps, together with impaired repair mechanisms, renders cells vulnerable to additional alterations in gap repair, such as in scenarios lacking long-range resection factors or when TLS is inhibited.

way PrimPol is recruited to long ssDNA stretches at stalled forks, which relies on its interaction with RPA (64,65). Alternatively, HU treatment can induce base damage by generating reactive oxygen species (66).

In addition, we found that proper ATR checkpoint activation upon MMS-induced replicative stress depends on the interaction between EXO1 and the DNA replication clamp PCNA. This interaction could facilitate the recruitment of EXO1 at sites of DNA damage and/or stimulate its processivity, mirroring observations seen in response to DSBs (40). Importantly, while PCNA is specifically loaded at the 3′-junction of the gap, EXO1 possess 5′-3′ exonuclease as well as 5′ structure-specific DNA endonuclease activities (67–69). Therefore, to accommodate the biochemical properties of both proteins, one might speculate that EXO1 could reach the 5′-junction of the gap if a ssDNA loop is formed, similar to those observed during the DNA end processing of DSBs, as well as in the context of base excision repair (70,71).

Apart from stimulating full ATR activation, the generation of ssDNA gaps appears to be required for the TS branch of DDT. Supporting the notion of gap-associated TS, research by Branzei *et al.* demonstrated that strand invasion initiated from ssDNA gaps rather than DNA ends (72). In addition, previous studies in yeast and mammalian cells uncovered a role of EXO1 in TS, consistent with the idea that gap expansion might be necessary for efficient strand invasion (10,19,23,31,55,56,73). In line with these findings, we propose a model for the error-free TS branch of DDT, which requires PrimPol for the generation of ssDNA gaps behind the fork, and necessitate the subsequent expansion of these gaps, achieved through the concerted actions of BRCA1 and the nucleases EXO1 and DNA2 (Figure 7).

Remarkably, additional impairment of gap filling upon inhibition of TLS by the loss of REV1-Polζ or POLQ has been shown to reduce the viability of BRCA1/2-mutant cells (21,33–36). Similarly, we observed that *exo1* cells exhibited significant sensitivity to the inhibition of the REV1-Polζ-dependent TLS. TLS polymerases are known to facilitate continuous DNA synthesis, thus limiting the accumulation of gaps induced by factors such as replication stress, oncogenes, or chemotherapy (21). Consequently, TLS inhibitors not only synergizes with gap-inducing conditions but also with other gap-filling pathways, highlighting their potential in cancer therapy since gaps have been identified as a cancer vulnerability (38,74). Given the association of EXO1 mutations with numerous cancer types (58), the inhibition of TLS could potentially offer therapeutic benefits in treating these cancers.

Strikingly, we revealed a synthetically lethal interaction between BRCA1 and EXO1, as recently published by Kooij *et al.* (75), as well as between BRCA1 and DNA2. Recent studies have suggested that distinct BRCA1 functions prevent the toxic accumulation of ssDNA gaps. For instance, gaps have been proposed to arise in BRCA1-deficient cells due to defects in Okazaki fragment processing (26). More recently, we collaborated in a study that found that BRCA1, when partnered with BARD1, facilitates continuous DNA synthesis in unchallenged conditions by directly ubiquitylating PCNA (37). Furthermore, BRCA1 has been shown to allow the process of gap filling by safeguarding gap integrity, through the restriction of MRE11 activity (8). Interestingly, we also found that BRCA1 has a role in facilitating ssDNA gap expansion. Therefore, it appears that the combined effects of gap accumulation and impaired gap repair render BRCA1-mutant cells vulnerable to additional alterations in gap repair processes, such as in scenarios lacking long-range resection factors or when TLS is inhibited (Figure 7). In line with this model, loss of 53BP1, which has been shown to restore HR and prevents gap accumulation in BRCA1-mutant cells (26,76), fully restored viability of EXO1 and BRCA1-deficient cells (75). Intriguingly, we discovered that the absence of either EXO1 or DNA2 did not result in synthetic lethality in the context of BRCA2 deficiency, even though gaps also accumulate in BRCA2-deficient cells when exposed to replicative stress (32). This observation might be attributed to the fact that, while both BRCA1 and BRCA2 are crucial for HR, it is BRCA1, and not BRCA2, that facilitates resection (57), in agreement with our own findings regarding ATR activation in BRCA mutants. Remarkably, we found that EXO1 is upregulated in BRCA1-deficient cells, and gene expression levels of *EXO1*, *DNA2* and *BLM* are elevated in tumor samples with very low *BRCA1* expression. These observations suggest the activation of a compensatory mechanism involving long-range resection in BRCA1-mutant cells. Accordingly, BLM, which cooperates with the nuclease DNA2 during long-range resection, has also been found to be essential in BRCA1-deficient but not in BRCA1-proficient cells (75). Noteworthy, EXO1 might also play a role in facilitating

the recruitment of TLS polymerases, as demonstrated for Polι and Polκ at ssDNA gaps intermediates generated during nucleotide excision repair (77). In any case, the accumulation of unrepaired ssDNA gaps can potentially lead to the formation of cytotoxic DSBs mediated by, for instance, the endonuclease activity of MRE11 (8,78). Importantly, we showed an additive effect of the loss of EXO1 and the inhibition of the REV1-Polζ-dependent TLS in the survival of BRCA1-deficient cells. Thus, our findings suggests that BRCA1-mutant patients might benefit from combinational therapies incorporating inhibitors targeting gap repair processes, including those associated with TLS polymerases or DNA2/EXO1.

Data availability

The data underlying this article are available in the article and in its online supplementary material. Raw data will be shared on reasonable request to the corresponding authors.

Supplementary data

Supplementary Data are available at NAR Online.

Acknowledgements

We thank Lene J. Rasmussen for kindly providing the YFP-EXO1 plasmid.

Author contributions: N.G.-R.: Conceptualization, Investigation, Formal Analysis, Writing (original draft), Writing (review and editing), Funding Acquisition. I.D.-G.: Investigation, Formal Analysis. MdC. D.-P.: Investigation. P.H.: Writing (review and editing), Funding Acquisition, Supervision.

Funding

Marie Skolodowska-Curie Fellowship from the European Union's Horizon 2020 Programme [MSCA-IF-2017-794054]; EMERGIA 2021 program from the Andalusian Regional Government-Junta de Andalucía [EMC21_00057 to N.G.-R.]; work in the laboratory of PH was funded by a grant from the Spanish Ministry of Science and Innovation [PID2019-104195G]. Funding for open access charge: Universidad de Sevilla.

Conflict of interest statement

None declared.

References

1. Zeman,M.K. and Cimprich,K.A. (2014) Causes and consequences of replication stress. *Nat. Cell Biol.*, **16**, 2–9.
2. Zou,L. and Elledge,S.J. (2003) Sensing DNA damage through ATRIP recognition of RPA-ssDNA complexes. *Science*, **300**, 1542–1548.
3. Maréchal,A. and Zou,L. (2013) DNA damage sensing by the ATM and ATR kinases. *Csh Perspect. Biol.*, **5**, a012716.
4. Quinet,A., Tirman,S., Cybulla,E., Meroni,A. and Vindigni,A. (2021) To skip or not to skip: choosing repriming to tolerate DNA damage. *Mol. Cell*, **81**, 649–658.
5. Friedberg,E.C. (2005) Suffering in silence: the tolerance of DNA damage. *Nat. Rev. Mol. Cell Biol.*, **6**, 943–953.
6. Sale,J.E. (2013) Translesion DNA synthesis and mutagenesis in eukaryotes. *Cold Spring Harb. Perspect. Biol.*, **5**, a012708.
7. Vaisman,A. and Woodgate,R. (2017) Translesion DNA polymerases in eukaryotes: what makes them tick? *Crit. Rev. Biochem. Mol. Biol.*, **52**, 274–303.
8. Tirman,S., Quinet,A., Wood,M., Meroni,A., Cybulla,E., Jackson,J., Pegoraro,S., Simoneau,A., Zou,L. and Vindigni,A. (2021) Temporally distinct post-replicative repair mechanisms fill PRIMPOL-dependent ssDNA gaps in human cells. *Mol. Cell*, **81**, 4026–4040.
9. Daigaku,Y., Davies,A.A. and Ulrich,H.D. (2010) Ubiquitin-dependent DNA damage bypass is separable from genome replication. *Nature*, **465**, 951–955.
10. Karras,G., Fumasoni,M., Sienski,G., Vanoli,F., Branzei,D. and Jentsch,S. (2013) Noncanonical role of the 9-1-1 clamp in the error-free DNA damage tolerance pathway. *Mol. Cell*, **49**, 536–546.
11. Karras,G.I. and Jentsch,S. (2010) The RAD6 DNA damage tolerance pathway operates uncoupled from the replication fork and is functional beyond S phase. *Cell*, **141**, 255–267.
12. Lehmann,A.R. (1972) Postreplication repair of DNA in ultraviolet-irradiated mammalian cells. *J. Mol. Biol.*, **66**, 319–337.
13. Prakash,L. (1981) Characterization of postreplication repair in *Saccharomyces cerevisiae* and effects of rad6, rad18, rev3 and rad52 mutations. *Mol. Gen. Genet.*, **184**, 471–478.
14. Lopes,M., Foiani,M. and Sogo,J.M. (2006) Multiple mechanisms control chromosome integrity after replication fork uncoupling and restart at irreparable UV lesions. *Mol. Cell*, **21**, 15–27.
15. Fumasoni,M., Zwicky,K., Vanoli,F., Lopes,M. and Branzei,D. (2015) Error-free DNA damage tolerance and sister chromatid proximity during DNA replication rely on the Polα/Primase/Ctf4 Complex. *Mol. Cell*, **57**, 812–823.
16. Bianchi,J., Rudd,S.G., Jozwiakowski,S.K., Bailey,L.J., Soura,V., Taylor,E., Stevanovic,I., Green,A.J., Stracker,T.H., Lindsay,H.D., *et al.* (2013) PrimPol bypasses UV photoproducts during eukaryotic chromosomal DNA replication. *Mol. Cell*, **52**, 566–573.
17. García-Gómez,S., Reyes,A., Martínez-Jiménez,M.I., Chocrón,E.S., Mourón,S., Terrados,G., Powell,C., Salido,E., Méndez,J., Holt,I.J., *et al.* (2013) PrimPol, an archaic primase/polymerase operating in human cells. *Mol. Cell*, **52**, 541–553.
18. Mourón,S., Rodriguez-Acebes,S., Martínez-Jiménez,M.I., García-Gómez,S., Chocrón,S., Blanco,L. and Méndez,J. (2013) Repriming of DNA synthesis at stalled replication forks by human PrimPol. *Nat. Struct. Mol. Biol.*, **20**, 1383–1389.
19. Wong,R.P., García-Rodríguez,N., Zilio,N., Hanulová,M. and Ulrich,H.D. (2020) Processing of DNA polymerase-blocking lesions during genome replication is spatially and temporally segregated from replication forks. *Mol. Cell*, **77**, 3–16.
20. Zellweger,R., Dalcher,D., Mutreja,K., Berti,M., Schmid,J.A., Herrador,R., Vindigni,A. and Lopes,M. (2015) Rad51-mediated replication fork reversal is a global response to genotoxic treatments in human cells. *J. Cell Biol.*, **208**, 563–579.
21. Nayak,S., Calvo,J.A., Cong,K., Peng,M., Berthiaume,E., Jackson,J., Zaino,A.M., Vindigni,A., Hadden,M.K. and Cantor,S.B. (2020) Inhibition of the translesion synthesis polymerase REV1 exploits replication gaps as a cancer vulnerability. *Sci. Adv.*, **6**, eaaz7808.
22. Elvers,I., Johansson,F., Groth,P., Erixon,K. and Helleday,T. (2011) UV stalled replication forks restart by re-priming in human fibroblasts. *Nucleic Acids Res.*, **39**, 7049–7057.
23. Piberger,A.L., Bowry,A., Kelly,R.D.W., Walker,A.K., González-Acosta,D., Bailey,L.J., Doherty,A.J., Méndez,J., Morris,J.R., Bryant,H.E., *et al.* (2020) PrimPol-dependent single-stranded gap formation mediates homologous recombination at bulky DNA adducts. *Nat. Commun.*, **11**, 5863.
24. Quinet,A., Tirman,S., Jackson,J., Šviković,S., Lemaçon,D., Carvajal-Maldonado,D., González-Acosta,D., Vessoni,A.T., Cybulla,E., Wood,M., *et al.* (2020) PRIMPOL-mediated adaptive response suppresses replication fork reversal in BRCA-deficient cells. *Mol. Cell*, **77**, 461–474.

25. González-Acosta,D., Blanco-Romero,E., Ubieto-Capella,P., Mutreja,K., Míguez,S., Llanos,S., García,F., Muñoz,J., Blanco,L., Lopes,M., *et al.* (2021) PrimPol-mediated repriming facilitates replication traverse of DNA interstrand crosslinks. *EMBO J.*, **40**, e106355.
26. Cong,K., Peng,M., Kousholt,A.N., Lee,W.T.C., Lee,S., Nayak,S., Krais,J., VanderVere-Carozza,P.S., Pawelczak,K.S., Calvo,J., *et al.* (2021) Replication gaps are a key determinant of PARP inhibitor synthetic lethality with BRCA deficiency. *Mol. Cell*, **81**, 3128–3144.
27. Bai,G., Kermi,C., Stoy,H., Schiltz,C.J., Bacal,J., Zaino,A.M., Hadden,M.K., Eichman,B.F., Lopes,M. and Cimprich,K.A. (2020) HLTF promotes fork reversal, limiting replication stress resistance and preventing multiple mechanisms of unrestrained DNA synthesis. *Mol. Cell*, **78**, 1237–1251.
28. Šviković,S., Crisp,A., Tan-Wong,S.M., Guilliam,T.A., Doherty,A.J., Proudfoot,N.J., Guilbaud,G. and Sale,J.E. (2019) R-loop formation during S phase is restricted by PrimPol-mediated repriming. *EMBO J.*, **38**, e99793.
29. Tercero,J., Longhese,M. and Diffley,J. (2003) A central role for DNA replication forks in checkpoint activation and response. *Mol. Cell*, **11**, 1323–1336.
30. Shimada,K., Pasero,P. and Gasser,S.M. (2002) ORC and the intra-S-phase checkpoint: a threshold regulates Rad53p activation in S phase. *Genes Dev.*, **16**, 3236–3252.
31. García-Rodríguez,N., Morawska,M., Wong,R.P., Daigaku,Y. and Ulrich,H.D. (2018) Spatial separation between replisome- and template-induced replication stress signaling. *EMBO J.*, **37**, e98369.
32. Panzarino,N.J., Krais,J.J., Cong,K., Peng,M., Mosqueda,M., Nayak,S.U., Bond,S.M., Calvo,J.A., Doshi,M.B., Bere,M., *et al.* (2021) Replication gaps underlie BRCA deficiency and therapy response. *Cancer Res.*, **81**, 1388–1397.
33. Taglialatela,A., Leuzzi,G., Sannino,V., Cuella-Martin,R., Huang,J.-W., Wu-Baer,F., Baer,R., Costanzo,V. and Ciccia,A. (2021) REV1-Polζ maintains the viability of homologous recombination-deficient cancer cells through mutagenic repair of PRIMPOL-dependent ssDNA gaps. *Mol. Cell*, **81**, 4008–4025.
34. Belan,O., Sebald,M., Adamowicz,M., Anand,R., Vancevska,A., Neves,J., Grinkevich,V., Hewitt,G., Segura-Bayona,S., Bellelli,R., *et al.* (2022) POLQ seals post-replicative ssDNA gaps to maintain genome stability in BRCA-deficient cancer cells. *Mol. Cell*, **82**, 4664–4680.
35. Schrempf,A., Bernardo,S., Verge,E.A.A., Otero,M.A.R., Wilson,J., Kirchhofer,D., Timelthaler,G., Ambros,A.M., Kaya,A., Wieder,M., *et al.* (2022) POLθ processes ssDNA gaps and promotes replication fork progression in BRCA1-deficient cells. *Cell Rep.*, **41**, 111716.
36. Mann,A., Ramirez-Otero,M.A., Antoni,A.D., Hanthi,Y.W., Sannino,V., Baldi,G., Falbo,L., Schrempf,A., Bernardo,S., Loizou,J., *et al.* (2022) POLθ prevents MRE11-NBS1-CtIP-dependent fork breakage in the absence of BRCA2/RAD51 by filling lagging-strand gaps. *Mol. Cell*, **82**, 4218–4231.
37. Salas-Lloret,D., García-Rodríguez,N., Giebel,L., Ru,A.d., Veelen,P.A.v., Huertas,P., Vertegaal,A.C.O. and González-Prieto,R. (2023) BRCA1/BARD1 ubiquitinates PCNA in unperturbed conditions to promote replication fork stability and continuous DNA synthesis. bioRxiv doi: https://doi.org/10.1101/2023.01.12.523782, 12 January 2023, preprint: not peer reviewed.
38. Cantor,S.B. (2021) Revisiting the BRCA-pathway through the lens of replication gap suppression "Gaps determine therapy response in BRCA mutant cancer." *DNA Repair (Amst.)*, **107**, 103209.
39. Liberti,S.E., Andersen,S.D., Wang,J., May,A., Miron,S., Perderiset,M., Keijzers,G., Nielsen,F.C., Charbonnier,J.-B.B., Bohr,V.A., *et al.* (2011) Bi-directional routing of DNA mismatch repair protein human exonuclease 1 to replication foci and DNA double strand breaks. *DNA Repair (Amst.)*, **10**, 73–86.
40. Chen,X., Paudyal,S.C., Chin,R.-I. and You,Z. (2013) PCNA promotes processive DNA end resection by Exo1. *Nucleic Acids Res.*, **41**, 9325–9338.
41. Guzmán,C., Bagga,M., Kaur,A., Westermarck,J. and Abankwa,D. (2014) ColonyArea: an ImageJ plugin to automatically quantify colony formation in clonogenic assays. *PLoS One*, **9**, e92444.
42. Goldman,M.J., Craft,B., Hastie,M., Repečka,K., McDade,F., Kamath,A., Banerjee,A., Luo,Y., Rogers,D., Brooks,A.N., *et al.* (2020) Visualizing and interpreting cancer genomics data via the Xena platform. *Nat. Biotechnol.*, **38**, 675–678.
43. Tang,Z., Li,C., Kang,B., Gao,G., Li,C. and Zhang,Z. (2017) GEPIA: a web server for cancer and normal gene expression profiling and interactive analyses. *Nucleic Acids Res.*, **45**, W98–W102.
44. Quinet,A., Carvajal-Maldonado,D., Lemacon,D. and Vindigni,A. (2017) Chapter three DNA fiber analysis: mind the Gap!. *Methods Enzymol.*, **591**, 55–82.
45. Kobayashi,K., Guilliam,T.A., Tsuda,M., Yamamoto,J., Bailey,L.J., Iwai,S., Takeda,S., Doherty,A.J. and Hirota,K. (2016) Repriming by PrimPol is critical for DNA replication restart downstream of lesions and chain-terminating nucleosides. *Cell Cycle*, **15**, 1997–2008.
46. Gallo,D., Kim,T., Szakal,B., Saayman,X., Narula,A., Park,Y., Branzei,D., Zhang,Z. and Brown,G.W. (2019) Rad5 recruits error-prone DNA polymerases for mutagenic repair of ssDNA gaps on undamaged templates. *Mol. Cell*, **73**, 900–914.
47. Byun,T.S., Pacek,M., Yee,M., Walter,J.C. and Cimprich,K.A. (2005) Functional uncoupling of MCM helicase and DNA polymerase activities activates the ATR-dependent checkpoint. *Genes Dev.*, **19**, 1040–1052.
48. Branzei,D. and Foiani,M. (2009) The checkpoint response to replication stress. *DNA Repair (Amst.)*, **8**, 1038–1046.
49. Huertas,P. (2010) DNA resection in eukaryotes: deciding how to fix the break. *Nat. Struct. Mol. Biol.*, **17**, 11–16.
50. Hsiang,Y.H., Lihou,M.G. and Liu,L.F. (1989) Arrest of replication forks by drug-stabilized topoisomerase I-DNA cleavable complexes as a mechanism of cell killing by camptothecin. *Cancer Res.*, **49**, 5077–5082.
51. Schaetzlein,S., Chahwan,R., Avdievich,E., Roa,S., Wei,K., Eoff,R.L., Sellers,R.S., Clark,A.B., Kunkel,T.A., Scharff,M.D., *et al.* (2013) Mammalian Exo1 encodes both structural and catalytic functions that play distinct roles in essential biological processes. *Proc. Natl. Acad. Sci. U.S.A.*, **110**, E2470–E2479.
52. Cejka,P. (2015) DNA end resection: nucleases team up with the right partners to initiate homologous recombination. *J. Biol. Chem.*, **290**, 22931–22938.
53. Hashimoto,Y., Chaudhuri,A.R., Lopes,M. and Costanzo,V. (2010) Rad51 protects nascent DNA from Mre11-dependent degradation and promotes continuous DNA synthesis. *Nat. Struct. Mol. Biol.*, **17**, 1305–1311.
54. Liu,W., Zhou,M., Li,Z., Li,H., Polaczek,P., Dai,H., Wu,Q., Liu,C., Karanja,K.K., Popuri,V., *et al.* (2016) A selective small molecule DNA2 inhibitor for sensitization of human cancer cells to chemotherapy. *EBioMedicine*, **6**, 73–86.
55. García-Rodríguez,N., Wong,R.P. and Ulrich,H.D. (2018) The helicase Pif1 functions in the template switching pathway of DNA damage bypass. *Nucleic Acids Res.*, **46**, 8347–8356.
56. Vanoli,F., Fumasoni,M., Szakal,B., Maloisel,L. and Branzei,D. (2010) Replication and recombination factors contributing to recombination-dependent bypass of DNA lesions by template switch. *PLos Genet.*, **6**, e1001205.
57. Prakash,R., Zhang,Y., Feng,W. and Jasin,M. (2015) Homologous recombination and human health: the roles of BRCA1, BRCA2, and associated proteins. *Cold Spring Harb. Perspect. Biol.*, **7**, a016600.
58. Keijzers,G., Bakula,D., Petr,M.A., Madsen,N.G., Teklu,A., Mkrtchyan,G., Osborne,B. and Scheibye-Knudsen,M. (2018) Human exonuclease 1 (EXO1) regulatory functions in DNA replication with putative roles in cancer. *Int. J. Mol. Sci.*, **20**, 74.

59. Giannattasio,M., Follonier,C., Tourrière,H., Puddu,F., Lazzaro,F., Pasero,P., Lopes,M., Plevani,P. and Muzi-Falconi,M. (2010) Exo1 competes with repair synthesis, converts NER intermediates to long ssDNA gaps, and promotes checkpoint activation. *Mol. Cell*, **40**, 50–62.
60. Zhu,Z., Chung,W.-H.H., Shim,E.Y., Lee,S.E. and Ira,G. (2008) Sgs1 helicase and two nucleases Dna2 and Exo1 resect DNA double-strand break ends. *Cell*, **134**, 981–994.
61. Dewar,J.M. and Lydall,D. (2010) Pif1- and Exo1-dependent nucleases coordinate checkpoint activation following telomere uncapping. *EMBO J.*, **29**, 4020–4034.
62. Tomimatsu,N., Mukherjee,B., Harris,J.L., Boffo,F.L., Hardebeck,M.C., Potts,P.R., Khanna,K.K. and Burma,S. (2017) DNA-damage-induced degradation of EXO1 exonuclease limits DNA end resection to ensure accurate DNA repair. *J. Biol. Chem.*, **292**, 10779–10790.
63. Meroni,A., Wells,S.E., Fonseca,C., Chaudhuri,A.R., Caldecott,K.W. and Vindigni,A. (2024) DNA combing versus DNA spreading and the separation of sister chromatids. *J. Cell Biol.*, **223**, e202305082.
64. Guilliam,T.A., Brissett,N.C., Ehlinger,A., Keen,B.A., Kolesar,P., Taylor,E.M., Bailey,L.J., Lindsay,H.D., Chazin,W.J. and Doherty,A.J. (2017) Molecular basis for PrimPol recruitment to replication forks by RPA. *Nat. Commun.*, **8**, 15222.
65. Wan,L., Lou,J., Xia,Y., Su,B., Liu,T., Cui,J., Sun,Y., Lou,H. and Huang,J. (2013) hPrimpol1/CCDC111 is a human DNA primase-polymerase required for the maintenance of genome integrity. *EMBO Rep.*, **14**, 1104–1112.
66. Somyajit,K., Gupta,R., Sedlackova,H., Neelsen,K.J., Ochs,F., Rask,M.-B., Choudhary,C. and Lukas,J. (2017) Redox-sensitive alteration of replisome architecture safeguards genome integrity. *Science*, **358**, 797–802.
67. Moldovan,G.-L.L., Pfander,B. and Jentsch,S. (2007) PCNA, the maestro of the replication fork. *Cell*, **129**, 665–679.
68. Wilson,D.M., Coleman,M.A., Adamson,A.W., Christensen,M., Lamerdin,J.E. and Carney,J.P. (1998) Hex1: a new human Rad2 nuclease family member with homology to yeast exonuclease 1. *Nucleic Acids Res.*, **26**, 3762–3768.
69. Lee,B.-I. and Wilson,D.M. (1999) The RAD2 domain of human exonuclease 1 exhibits 5′ to 3′ exonuclease and Flap structure-specific endonuclease activities. *J. Biol. Chem.*, **274**, 37763–37769.
70. Yoo,J., Lee,D., Im,H., Ji,S., Oh,S., Shin,M., Park,D. and Lee,G. (2021) The mechanism of gap creation by a multifunctional nuclease during base excision repair. *Sci. Adv.*, **7**, eabg0076.
71. Xue,C., Salunkhe,S.J., Tomimatsu,N., Kawale,A.S., Kwon,Y., Burma,S., Sung,P. and Greene,E.C. (2022) Bloom helicase mediates formation of large single–stranded DNA loops during DNA end processing. *Nat. Commun.*, **13**, 2248.
72. Giannattasio,M., Zwicky,K., Follonier,C., Foiani,M., Lopes,M. and Branzei,D. (2014) Visualization of recombination-mediated damage bypass by template switching. *Nat. Struct. Mol. Biol.*, **21**, 884–892.
73. Tran,P.T., Fey,J.P., Erdeniz,N., Gellon,L., Boiteux,S. and Liskay,R. (2007) A mutation in EXO1 defines separable roles in DNA mismatch repair and post-replication repair. *DNA Repair (Amst.)*, **6**, 1572–1583.
74. Patel,S.M., Dash,R.C. and Hadden,M.K. (2021) Translesion synthesis inhibitors as a new class of cancer chemotherapeutics. *Expert Opin. Investig. Drugs*, **30**, 13–24.
75. Kooij,B.v., Schreuder,A., Pavani,R., Garzero,V., Uruci,S., Wendel,T.J., Hoeck,A.v., Alonso,M.S.M., Everts,M., Koerse,D., *et al.* (2024) EXO1 protects BRCA1-deficient cells against toxic DNA lesions. *Mol. Cell.*, **84**, 659–674.
76. Bunting,S.F., Callén,E., Wong,N., Chen,H.-T., Polato,F., Gunn,A., Bothmer,A., Feldhahn,N., Fernandez-Capetillo,O., Cao,L., *et al.* (2010) 53BP1 inhibits homologous recombination in Brca1-deficient cells by blocking resection of DNA breaks. *Cell*, **141**, 243–254.
77. Sertic,S., Mollica,A., Campus,I., Roma,S., Tumini,E., Aguilera,A. and Muzi-Falconi,M. (2018) Coordinated activity of Y family TLS polymerases and EXO1 protects non-S phase cells from UV-induced cytotoxic lesions. *Mol. Cell*, **70**, 34–47.
78. Hale,A., Dhoonmoon,A., Straka,J., Nicolae,C.M. and Moldovan,G.-L. (2023) Multi-step processing of replication stress-derived nascent strand DNA gaps by MRE11 and EXO1 nucleases. *Nat. Commun.*, **14**, 6265.

Received: October 6, 2023. **Revised:** March 25, 2024. **Editorial Decision:** April 9, 2024. **Accepted:** May 2, 2024